A comparative study on the effects of blast actions on a monumental structure

P. Vannucci, Filippo Masi, Ioannis Stefanou

A comparative study on the effects of blast actions on a monumental structure

P. Vannucci*[1], F. Masi[2], and I. Stefanou[2]

[1]LMV, Laboratoire de Mathématiques de Versailles - UMR8100 CNRS & UVSQ.
Université Paris-Saclay, Versailles (F)

[2]Laboratoire Navier - UMR8205, CNRS, ENPC & IFSTTAR.
Université Paris-Est, Marne La Vallée (F)

July 19, 2018

Abstract

The problem of evaluating the effects of an explosion inside a monumental building is addressed; namely, we focus on the determination of the overpressure due to the shock wave. Three models are compared: a thermodynamic approach, based on the JWL model and two empirical approaches, based on the CONWEP method or the recommendations TM5-1300, both of them approaches proposed by USACE.

In particular, a detailed procedure for the use of TM5-1300 is proposed, making use of new analytical expressions of the physical parameters of a hemispherical blast fitting the experimental data of Kingery and Bulmash. The novelty of these expressions is that they fit accurately the experimental data over the entire variation range of the scaled distance.

In the paper, we show the existence of reflected waves focus, a phenomenon that alters sensibly the pressure field in case of non-typical geometries, like vaults or domes. We show that for this kind of structures the assessment of the blast effects is adequately estimated by the JWL method, while in the case of more typical, planar geometries, namely of flat walls, the assessment of the overpressure is sufficiently estimated also by TM5-1300.

Key words: blast actions, fast dynamics, architectural monuments.

1 Introduction

The most widely used methods for the evaluation of the actions and effects of a blast on a civil structure are based upon the use of empirical laws, i.e. on laws describing the main physical quantities related to an explosion, that have been obtained as the result

*Corresponding author: Paolo Vannucci. LMV, 45 Avenue des Etats-Unis. 78035 Versailles, France
E-mail: paolo.vannucci@uvsq.fr

of experimental measurements. Such an approach has the advantage of being relatively simple to be used in calculations by hand or in numerical procedures, at least when the geometry of the blast scenario (i.e. the geometry of the constructions affected by the blast) is not too complicated.

The use of empirical laws has been widely studied and coded in different recommendations/rules, mostly proposed by military authorities. In particular, the two most commonly used empirical models are based upon different but related studies of the U.S. Army Corps of Engineers (USACE): the document [USACE, 1986], containing the model CONWEP, and the Technical Manual TM5-1300, [USACE, 1990], completed by successive documents, [USACE, 2008]. The Joint Research Center of the European Union has produced in 2013 a Technical Report, [Karlos and Solomos, 2013], substantially referring to these two last documents and to another Technical Report of the U.S. Army, [Kingery and Bulmash, 1984]. In [Karlos and Solomos, 2013] all the empirical laws of [USACE, 1990] are reproduced using S. I. units.

In particular, TM5-1300 recommendations contain several indications for the calculation of the physical parameters of a blast in different scenarios, for both the cases of an explosion outside or inside a building. Unfortunately, such scenarios are related to relatively simple and recurrent geometries, so such indications/practical computation schemes are not suited in more uncommon situations.

The case of monumental structures is one of those possible unusual scenarios. In fact, the geometry of monuments such as old palaces, cathedrals, temples and so on is more complicated and articulated than simple box-shaped building, like those considered in technical recommendations. In such cases, the scenario cannot be reduced to one of the cases provided by technical rules like TM5-1300.

Another aspect can be of great importance in the case of a blast inside a monument. The peculiar geometry of certain structural elements like vaults, domes, absides can produce a physical phenomenon that is not included in the empirical rules: the reflection and focusing of shock waves. This effect is described in this paper on a simple example representing a possible, common monumental structure, i.e. a barrel-vaulted hall. We show that it can have a great importance in the analysis of the effects of a blast on a monumental structure. Reflected shock waves are not taken into account by empirical methods. However, the effects of reflected waves, especially in the case of internal blasts, can be very important and generally speaking, not negligible.

The use of empirical approaches to the study of the effects of a blast on a monumental structure, especially for the case of internal explosions, may therefore be inappropriate. Approaches based upon a complete, more physical, description of the blast are preferable. Such methods, the most well known being the so-called JWL model, are based upon the laws of thermodynamics to recover the physics of a chemical blast; they allow for a complete description of the phenomenon of the blast, including the propagation of reflected shock waves. The drawback of such approaches is that usually they need heavy numerical simulations.

The study of the effects of a blast on a monumental structure has acquired today great importance: architectural monuments of the past, as symbols of a cultural heritage proper to a nation, to a civilization or to a religion, have been unfortunately too often the objects

of violences and iconoclastic destructions. The examples of the Cathedral of Reims in 1914, the Buddha statues of Bamyan in 2001 and the more recent destructions at Palmyra in 2015 and 2016 or at Mosul in 2017 are just some few recent examples of that.

The present international situation has brought to the attention of people and governments the threat on highly representative monuments, that can be today the target of destructive attacks. It is hence relevant to consider the mechanical problem of the effects of a blast on a monumental structure; rather surprisingly, literature seems poor about this matter. The most part of papers concerning the effects of an explosion on a civil structure regard reinforced concrete structures and usually the geometries considered are really simple, normally a squared building, [Remennikov, 2003], [Ngo et al., 2007], [Koccaz et al., 2008], [Draganic and Sigmund, 2012], in some cases bridges, e.g. [Birhane, 2009]. As mentioned above, this is seldom the case of architectures of the past, often much more articulated than simple squared buildings.

In this paper, we ponder on the best way to study the effects of a blast inside a monumental structure. We compare, to this purpose, different approaches: one based upon the use of JWL so giving a detailed description of the phenomenon, including the reflected waves. Then, three other approaches are used: one using the CONWEP method, [USACE, 1986], another using the approach suggested by the Technical Manual TM5-1300, [USACE, 1990] and finally a last one combining these two last approaches.

The approaches based upon the JWL and CONWEP methods have been used as implemented in finite element codes. For what concerns the method based upon the TM5-1300 recommandations, we propose in this paper an approach, namely a sequence of calculation, which is new and that is based upon a new analytical representation of the empirical data describing the different parameters of a hemispherical blast. This analytical representation is accurate and allows to represent by a unique function each physical parameter (namely, incident and reflected pressure and impulse, arrival time and duration of the positive phase, see Sect. 4). This can lead to a more elegant and straightforward implementation of the aforementioned empirical models in software for structural analyses.

The paper is subdivided into six Sections: the first one, Sect. 2, is devoted to a general description of the mechanical effects of a blast (we do not consider in this paper thermal effects nor the projection of fragments). The JWL model, [Jones and Miller, 1948], [Wilkins, 1964], [Lee et al., 1968], is shortly recalled in Sect. 3, while Sect. 4 is devoted to the empirical models for the calculation of the blast overpressure and to the new analytical representations for the different physical parameters. In Sect. 5 we propose a procedure for the evaluation of the blast overpressure, using precise interpolating functions of the experimental data contained in the report [USACE, 1990], while in Sect. 6 we give a brief account of the model CONWEP, [USACE, 1986]. Finally, a comparison of the three models is given in Sect. 7, in a case study representing schematically the interior of a possible monument. A last Sect. 8 giving the conclusions ends the paper.

2 The mechanical effects of a blast

An explosion is an extremely rapid and exothermic chemical reaction that lasts just few milliseconds. During detonation, hot gases, produced by this chemical reaction, expand

quickly and, for the hot temperatures produced instantaneously, the air around the blast expands too. The result is a blast shock wave, characterized by a thin zone of air propagating spherically much faster than the sound speed, through which pressure is discontinuous.

The shock-wave, travelling along a solid surface, produces an almost instantaneous increase of the air pressure on the surface, that decreases very quickly to the ambient pressure; this is the so-called positive phase of the blast. Then, the pressure decreases further, below the ambient pressure and then increases again to the ambient pressure, but in a longer time; this is the negative phase of the blast, see Fig. 1. The shock wave is the main mechanical effect of a blast on a structure, but not the only one: the hot gases, expanding, produce the so-called dynamic pressure, least in value with respect to the shock wave and propagating at a lower speed, while the impinging shock wave can be reflected by solid surfaces and act again on other surfaces as reflected shock wave.

To better understand all the mechanics of a blast, let us first introduce some quantities, used in the following:

- W: explosive mass;
- $R = ||q - o||$: distance of a point q from the detonation point o;
- P_o: ambient pressure;
- P_s: overpressure due to the blast; it is the pressure in the air relative to P_o;
- P_{so}: side-on overpressure peak: the shock-wave peak pressure, relative to P_o, measured in the air at q;
- P_r: reflected overpressure: the pressure, relative to P_o, acting at a point q of a solid surface when hit orthogonally by a shock-wave;
- P_{ro}: peak value of P_r;
- $P_{r\alpha}$: peak value of the reflected overpressure at a point q of a solid surface atilt of the angle α on the direction of $q - o$;
- t_A: arrival time, i.e. the instant at which the shock-wave peak arrives at q, taking as $t = 0$ the instant of detonation; of course, t_A increases with R, but experimental evidence has shown that it decreases with W, i.e. the velocity of the shock-wave increases with the quantity of explosive;
- t_o: positive phase duration; this is the duration of the time interval, starting from t_A, during which $P_s \geq 0$; t_o increases with R;
- t_{o-}: negative phase duration; this is the duration of the time interval, starting from $t_A + t_o$, during which $P_s < 0$;
- Z: Hopkinson-Cranz scaled distance, [Karlos and Solomos, 2013], defined as,

$$Z = \frac{R}{W^{\frac{1}{3}}}; \tag{1}$$

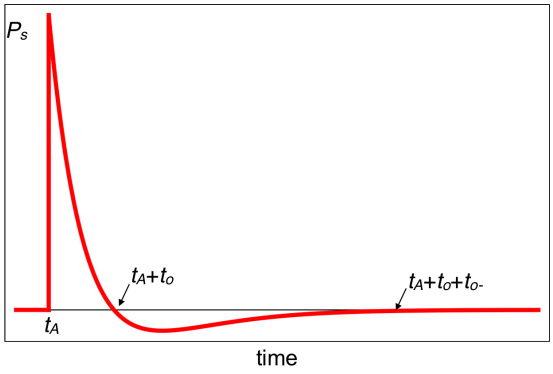

Figure 1: Scheme of the time variation of the pressure due to a blast.

- i_s: impulse of the shock-wave positive overpressure, defined as

$$i_s = \int_{t_A}^{t_A+t_o} P_s(q,t)\ dt; \tag{2}$$

- i_r: impulse of the shock-wave positive reflected overpressure, defined as

$$i_r = \int_{t_A}^{t_A+t_o} P_r(q,t)\ dt; \tag{3}$$

- t_{rf}: fictitious duration of the positive phase of the blast, defined as

$$t_{rf} = \frac{2\ i_r}{P_{ro}}; \tag{4}$$

- $t_{Aw},\ t_{ow},\ t_{ow-}$: scaled durations, obtained dividing the respective durations by $W^{\frac{1}{3}}$;
- $i_{sw},\ i_{rw}$: scaled impulses, obtained dividing the respective impulses by $W^{\frac{1}{3}}$.

The overpressure P_s at a point q decreases with both the time $t > t_A$ and R. Generally, the time rate decrease is much greater than the space rate decrease: the blast overpressure is really like a very localized pressure wave that propagates at high speed and whose intensity decreases, like for any other wave, with the travelled distance.

Fig. 1 represents an ideal profile of the overpressure $P_s(q,t)$. When the shock wave arrives at q, after t_A from detonation, the pressure instantaneously increases, from the ambient pressure P_o to a peak P_{so}, which is a strong discontinuity.

For $t > t_A$ the overpressure decreases extremely fast, with an exponential rate, until time $t_A + t_o$, the end of the positive phase. After $t_A + t_o$ we have the negative phase: the pressure decreases with respect to P_o and then it returns to P_o after a time $t_{o-} > t_o$. During the negative phase, the decrease of the pressure is much lower in absolute value, than the peak pressure of the positive phase. This is why the negative phase is usually neglected in structural analyses, even though it can be important in some specific cases, due to its duration, which is always much longer than the positive phase.

Generally, the arrival time t_A decreases, for the same distance R, when the amount of explosive W increases, i.e. the velocity of the shock-wave increases. The peak value P_{so},

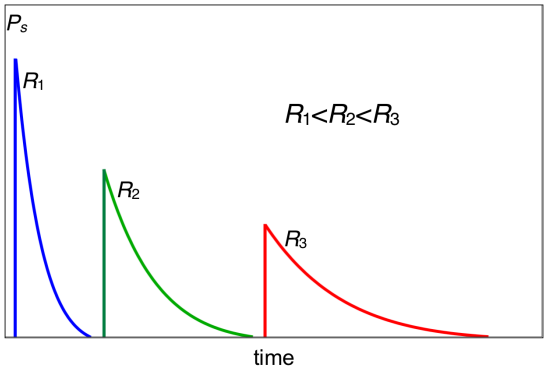

Figure 2: Influence of the distance R on the positive phase of a blast.

on its side, increases with W and decreases with R, while the time duration t_o does exactly the opposite, see Fig. 2.

The decrease of the pressure wave, i.e. the function $P_s(q,t)$, is an extremely rapid phenomenon; it can be modeled by the Friedlander's equation, [Karlos and Solomos, 2013]:

$$P_s(q,t) = P_{so}(q)\left(1 - \frac{t - t_A}{t_o}\right) e^{-b\frac{t-t_A}{t_o}}. \tag{5}$$

With this model, the impulse can be calculated analytically:

$$i_s(q,t) = P_{so}(q)\frac{t_o}{b^2}(b - 1 + e^{-b}). \tag{6}$$

This relation is useful for determining the decay coefficient b if i_s is known, e.g. from experimental data or with the method proposed below; a discussion about the value of b is given in Sect. 7.5. The same rate decrease (5) is used also for the reflected overpressure, P_r.

P_r is the pressure that acts on a surface impinged by the incident overpressure P_s. The peak P_{ro} of P_r is normally much greater than P_{so} measured at the same point in the absence of any surface. In fact, if we consider air as an ideal linear-elastic fluid, the air particles should bounce back freely from the surface, this giving a P_r equal to the double of the incident pressure. But normally, $P_{ro}/P_{so} > 2$ because a blast is actually a nonlinear shock phenomenon, where the reflection of the particles is hindered by subsequent air particles, with consequently a far higher reflected pressure.

A formula relating the values of P_{ro} and P_{so} for normal shocks is

$$P_{ro} = 2P_{so}\frac{4P_{so} + 7P_o}{P_{so} + 7P_o}, \tag{7}$$

The above equation indicates, on one side, that the ratio P_{ro}/P_{so} is not constant, but depends upon P_{so} and, on the other side, that this ratio can vary between 2 and 8 or more. Of course, it is the value of P_{ro} to be used for structural design. The Friedlander's law is used also for describing the decrease of P_r.

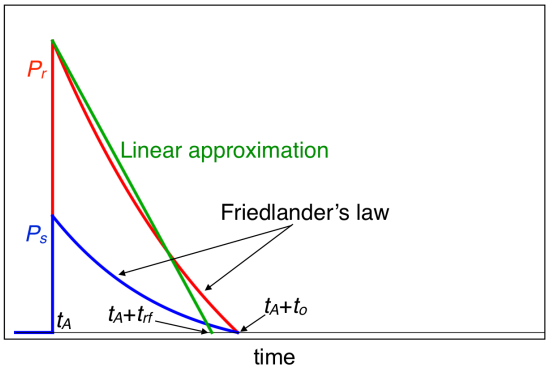

Figure 3: The Friedlander law.

Sometimes, the Friedlander's law is replaced by a simpler linear approximation, see Fig. 3. The fictitious positive duration time t_{rf} is then calculated imposing to preserve the same P_{ro} and i_r, which gives eq. (4).

The reflected pressure becomes, on its turn, an incident pressure for other surfaces, which of course complicates the situation: different incident waves can hit a surface besides the first one originated directly by detonation, all reflected by other surfaces, so giving a time history of the overpressure at a point that can have several successive peaks. In some cases, the effects of reflected waves can produce a peak of the overpressure greater than the one corresponding to the incident wave, especially in the case of a blast inside a building.

Another phenomenon produced by a blast is the dynamic pressure; the air behind the front of the blast wave moves like a wind, but with a smaller velocity. This wind causes a *dynamic* or *drag* pressure Q, loading a surface for the whole duration of the wind produced by the blast. Its peak value Q_o is less than P_{so} and it is delayed with respect to t_A, but Q has a much longer duration (up to $2 \div 3$ s) than t_o (some ms).

The blasts can be of different types: in *free-air bursts* the detonation occurs in the air and the blast waves propagate spherically outwards and impinge first and directly onto the structure, without prior interaction with other obstacles or the ground. In *air bursts* the detonation occurs still in the air but the overpressure wave arrives at the structure after having first interacted with the ground; a *Mach wave front* is created. *Surface bursts* are the explosions where detonation occurs almost at ground surface: the blast waves immediately interact locally with the ground and they propagate next hemispherically outwards and impinge onto the structure. Finally, in *internal blasts* the detonation occurs inside a structure: blast waves propagate and interact with the walls, reflected waves are generated and the effects of dynamic pressure due to gas expansion are amplified by the surrounding space.

In the case of explosions in monuments, we are concerned with surface blasts, i.e. with hemispherical overpressure waves. Surface blasts result in much greater shock overpressure than air-blasts, because of the ground effect that reflects and amplifies the overpressure wave.

The case of internal blasts is also important in the study of monuments; nevertheless, in several cases an internal blast can be considered as an external one. This happens for

buildings like churches or great halls, where the internal volume is so large to limit the effects of dynamic pressure and reflected waves.

The simulation of a blast can be conducted using different approaches, the most widely used being three: the JWL model, the CONWEP model and the TM5-1300 model. They are detailed in the following sections.

3 The JWL model

JWL stands for Jones, Wilkins and Lee, the authors of this model, [Jones and Miller, 1948], [Wilkins, 1964], [Lee et al., 1968]. Basically, JWL is a physically based model using the laws of thermodynamics to recover the physics of a chemical blast.

This model allows, in principle, to obtain a complete description of a blast phenomenon, i.e. including not only the propagation of the shock-wave in a medium, e.g. air, but also its reflection on solid surfaces and the expansion of the hot gases, i.e. the dynamic pressure. The JWL model is implemented in different commercial codes and its use needs the meshing not only of the structure, but also of the air volume involved in the blast.

The JWL model gives the overpressure P_s as function of different parameters:

$$P_s = A\left(1 - \frac{\omega\ \rho}{R_1\rho_0}\right)\exp\left(-R_1\frac{\rho_0}{\rho}\right) + B\left(1 - \frac{\omega\ \rho}{R_2\rho_0}\right)\exp\left(-R_2\frac{\rho_0}{\rho}\right) + \omega\ \rho\ E_m. \quad (8)$$

In the above equation, $A,\ B,\ R_1,\ R_2$ and ω are parameters depending upon the explosive, along with ρ_0, its density, while ρ is the density of the detonation products and E_m is the internal energy per unit mass. In addition, detonation velocity v_D and the Chapman-Jouguet pressure p_{cj} need to be specified. All the parameters are derived by fitting experimental results.

The use of JWL model allows a rather precise and complete simulation of the blast phenomenon, but its drawback is the need of discretising, finely, the charge and the fluid domain, that can be very large, besides the structure for the coupled structural analysis. Such multi-physics transient problems, with a strong coupling between fluid and structure dynamics, lead to numerical simulations that can be, in the case of a monument, very heavy, computationally speaking.

So this model, though in principle able to describe precisely the blast event and its mechanics, can be problematic to use in the case of monumental structures, where the fluid volume to discretize is very large.

4 Empirical models

Because of the drawbacks of the model JWL detailed hereon, empirical methods are more often used in calculations. They offer a good balance between computing cost and precision. These models are based upon the results of experimental tests and model uniquely the effects of the blast, namely the pressure field.

With such models, the characteristic parameters of the explosive serve to calculate the overpressure shock-wave and its propagation speed. The wave propagates spherically from the detonation point o to the elements of the structure. The distance of o from any impact point q on a surface of the structure and the inclination of the perpendicular to the surface with respect to the vector $q - o$ are the only geometric parameters needed by the models.

In fact, these models consider just the incident wave, not the reflected ones, nor the dynamic pressure. So, what is mainly lost with empirical models is the possibility of taking into account for the set of reflected waves that impinge again the wall surfaces.

Nevertheless, the effect of the reflection of the shock-wave by the ground, in the case of a ground-explosion, is taken into account by specific laws, different from those modeling a free-air burst: the models for hemispherical blasts differ from those for the spherical ones, the first ones giving higher values of the overpressure to take into account for the ground reflection and the formation of the so-called Mach stem.

This phenomenon is due to the reflection of the wave pressure by a surface. In general, the overpressure shock-wave due to an air detonation is produced by an incident wave, emanating from the explosive charge, and by a wave reflected, at least, by the ground. For small incident angles, up to about 40°, the incident wave is ahead of the reflected wave produced by the surface and typical reflection occurs. However, for larger angles, coalescence between the incident and the reflected wave takes place, creating a Mach stem.

In ground explosions, the interaction between the ground and the blast wave takes place since the beginning, due to the closeness of the detonation point to the ground surface. Instead of the creation of a Mach front at a certain distance from the detonation point, the incident wave is reflected immediately by the ground. This wave coalescence can give much greater pressure values than the normal reflection.

If the ground was a rigid surface, the reflected pressure P_r would be twice that of a free-air burst. In practice, a part of the energy is absorbed by the creation of a crater, so P_r is less than the double of a free-air burst pressure, say $1.7 \div 1.8$ times.

As said in the introduction, the two most commonly used empirical models are CONWEP, [USACE, 1986], and the Technical Manual TM5-1300, [USACE, 1990], completed by successive documents, [USACE, 2008],[Karlos and Solomos, 2013],

All these documents are based upon the experimental results contained in another Technical Report of the U.S. Army, [Kingery and Bulmash, 1984], which contains a large collection of numerical data measured during blast tests and universally accepted as reference experiments in blast analysis. Such data concern both the cases of spherical and hemispherical explosions and most important they provide the data not only for the incident pressure peak P_{so}, but also for the reflected one, P_{ro}, which is by far most interesting for design purposes.

In Fig. 4 we show the results of these experiments for what concerns the value of P_{so} and P_{ro} for hemispherical blasts. It is immediate to observe that P_{ro} is always greater than P_{so} for any Z.

The experimental data of Kingery and Bulmash for all the parameters of the positive

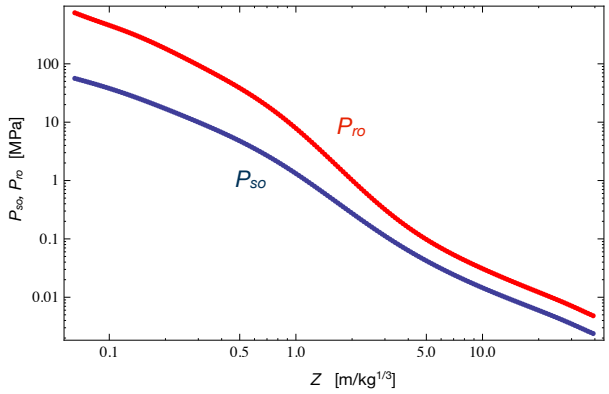

Figure 4: Results of the Kingery and Bulmash tests for P_{so} and P_{ro} (hemispherical blasts).

phase of a hemispherical blast are represented in Fig. 5. The diagrams are referred to the explosion of 1 kg of TNT and concern a distance range from 0.5 to 40 m. As they are given as functions of Z, it is possible to adapt such data also to other cases, by multiplying by $W^{\frac{1}{3}}$ the value of the scaled parameters, except for pressure and velocity.

4.1 New analytical expressions for the Kingery-Bulmash data

The experimental data of Kingery and Bulmash are the basis of the most common empirical methods. To this purpose, it is important to interpolate the experimental data. Several authors, starting from Kingery and Bulmash, have proposed analytical expressions fitting the data (see [Ullah et al., 2017] for a recent review). We consider here only the case of hemispherical blasts.

The original work of Kingery and Bulmash, [Kingery and Bulmash, 1984], gives the value of the logarithm base 10 of a physical parameter Y as a linear combination of powers of a function of the logarithm base 10 of Z:

$$\log(Y) = \sum_{j=0}^{n} c_j U^j, \quad U = k_0 + k_1 \log(Z). \tag{9}$$

Just for example, the values of the numerical coefficients n, c_j, k_0 and k_1 for some physical parameters are given in Tab. 1.

Swisdak, [Swisdak, 1994] has proposed alternative analytical representations for the experimental data of Kingery and Bulmash, namely of the form

$$\ln(Y) = \sum_{j=0}^{n} k_j Z^j; \tag{10}$$

unfortunately, such expressions do not cover the entire range of the scaled distance Z for the experiments, so the coefficients k_j are given for different sub-intervals of validity, see Tab. 2.

Several other analytical expressions have been proposed in the literature, for representing the Kingery and Bulmash experimental data or also other data; a rather exhaustive

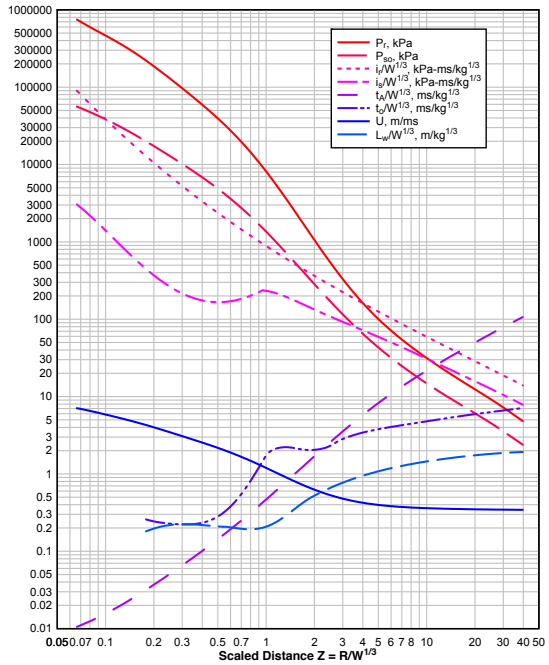

Figure 5: Blast parameters for the positive phase of a hemispherical blast, according to Kingery and Bulmash (from [Karlos and Solomos, 2013]).

list of them, for the different physical parameters, can be found in [Ullah et al., 2017]. However, the most precise expressions, when compared to the experimental results, are those proposed by Swisdak, eq. (10).

In view of an empirical approach, our purpose was to dispose of reliable, i.e. as much precise as possible, analytical representations of the Kingery and Bulmash data for P_{so}, P_{r_o}, i_{ow}, i_{rw}, t_{Aw} and t_{ow} valid for all the range of the data, i.e. for $Z \in [0.05, 40]$ m/kg$^{1/3}$. Therefore, we have limited the comparison just to the original data and to the corresponding diagrams obtained with eqs. (9), and (10). Such comparisons, along with the analytical expressions that we propose for different physical parameters of hemispherical blasts, are presented below. In all the diagrams presented below, the experimental data are represented by a series of blue dots, almost contiguous, while eq. (9) is represented by an orange curve and eq. (10) by a green one. The proposed analytical expressions are represented by red line; very often, the analytical expressions are so close to the empirical data that they are hard to be distinguished. It is shown that the proposed interpolations fit accurately the experimental data over the entire range of the scaled distance, contrary to the Swisdak [Swisdak, 1994] interpolation.

Incident pressure P_{so}:

$$P_{so} = \exp\big(0.26473 - 1.5168 \ln Z - 0.079822 \ln^2 Z - 0.57802 \sin(\ln Z) \\ -0.228409 \sin^2(\ln Z)\big)\,(1 + \frac{1}{2e^{10Z}}); \tag{11}$$

In Fig. 6 we show the comparison of the results given by eq. (11) with those given by eq. (9), eq. (10) and the experimental results.

Table 1: Coefficients for the fitting functions of Kingery and Bulmash (9), from [UNODA, 2015]. ΔZ: range of validity in terms of the scaled distance (1) [m/kg$^{1/3}$].

	P_{so}	P_{ro}	i_{sw}		i_{rw}
	[kPa]	[kPa]	[kPa ms/kg$^{1/3}$]		[kPa ms/kg$^{1/3}$]
ΔZ	0.05 ÷ 40	0.05 ÷ 40	0.0674 ÷ 0.955	0.955 ÷ 40	0.05 ÷ 40
n	8	9	4	7	3
k_0	-0.214362789151	-0.240657322658	2.06761908721	-1.94708846747	-0.246208804814
k_1	1.35034249993	1.36637719229	3.0760329666	2.40697745406	1.33422049854
c_0	2.78076916577	3.40283217581	2.52455620925	1.67281645863	2.70588058103
c_1	-1.6958988741	- 2.21030870597	- 0.502992763686	- 0.384519026965	- 0.949516092853
c_2	0.154159376846	0.218536586295	0.171335645235	- 0.0260816706301	0.112136118689
c_3	0.514060730593	0.895319589372	0.0450176963051	0.00595798753822	- 0.0250659183287
c_4	-0.0988534365274	0.24989009775	- 0.0118964626402	- 0.014544526107	
c_5	-0.293912623038	- 0.569249436807		- 0.00663289334734	
c_6	-0.0268112345019	0.11791682383		- 0.00284189327204	
c_7	0.109097496421	0.224131161411		0.0013644816277	
c_8	0.00162846756311	0.0245620259375			
c_9		- 0.455116002694			

Reflected pressure P_{ro}:

$$P_{ro} = \exp\left(2.03043 - 1.80367 \ln Z - 0.0929389 \ln^2 Z - 0.877952 \sin(\ln Z) - 0.360291 \sin^2(\ln Z)\right)\left(1 + \frac{1}{2e^{10Z}}\right). \tag{12}$$

The comparison of eq. (12) with eqs. (9) and (10) and the experimental data is shown in Fig. 7.

Scaled incident impulse i_{sw}:

$$i_{ow} = \exp\left(-2.11036 - 1.06541 \ln Z + 0.0733434 \ln^2 Z + 0.85168 \sin(\ln Z) - 0.0367758 \sin^3(\ln Z) + 0.512623 \cos(\ln Z)\right). \tag{13}$$

The comparison of eq. (12) with eqs. (9) and (10) and the experimental data is shown in Fig. 8.

Scaled reflected impulse i_{rw}:

$$i_{rw} = \exp\left(-0.110157 - 1.40609 \ln Z + 0.0847358 \ln^2 Z\right), \tag{14}$$

The comparison of eq. (12) with eqs. (9) and (10) and the experimental data is shown in Fig. 9.

Scaled arrival time t_{Aw}:

$$t_{Aw} = \exp\left(-0.684763 + 1.42884 \ln Z + 0.0290161 \ln^2 Z + 0.410838 \sin(\ln Z)\right), \tag{15}$$

The comparison of eq. (12) with eq. (10) and the experimental data is shown in Fig. 10.

Scaled duration time t_{ow}:

$$\begin{aligned} t_{ow} = \exp[&0.592314 + 2.91395 \ln Z - 1.28798 \ln^2 Z - 1.78825 \ln^3 Z \\ &+ 1.15091 \ln^4 Z + 0.325339 \ln^5 Z - 0.383478 \ln^6 Z \\ &+ 0.0903967 \ln^7 Z - 0.0044163 \ln^8 Z - 0.00046355 \ln^9 Z \\ &+ 0.537081 \cos^7(1.03191(\ln Z - 0.858947)) \sinh(1.08808(\ln Z - 2.02303))]. \end{aligned} \tag{16}$$

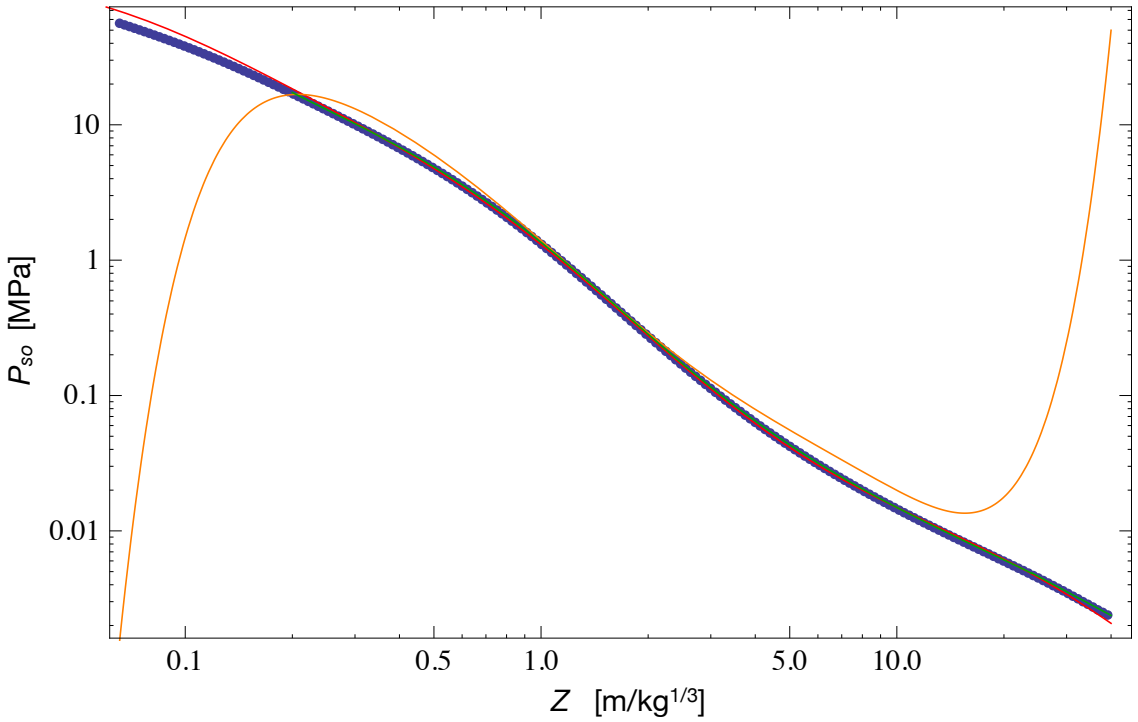

Figure 6: Comparison of experimental and fitted values of P_{so}.

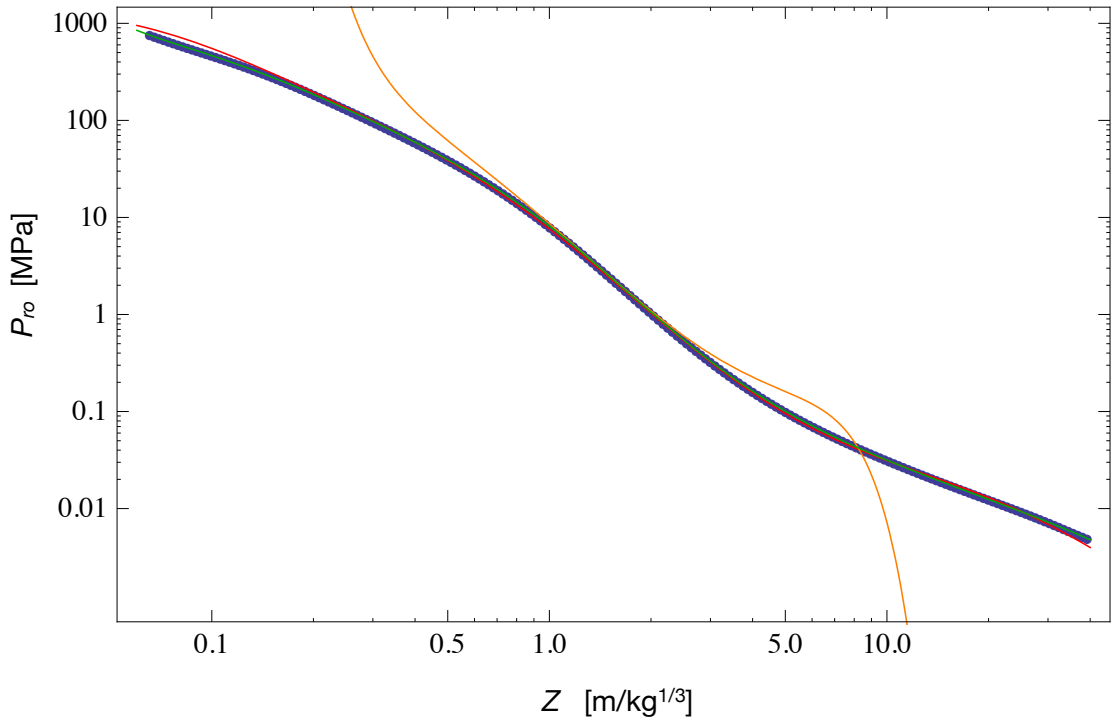

Figure 7: Comparison of experimental and fitted values of P_{ro}.

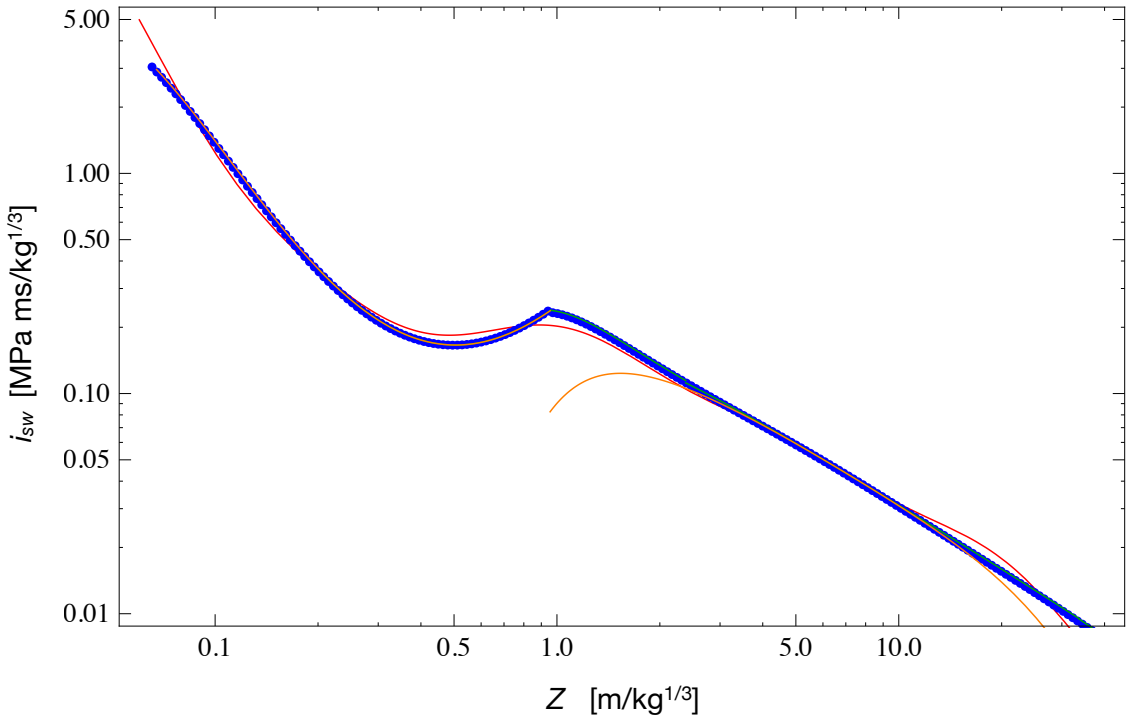

Figure 8: Comparison of experimental and fitted values of i_{sw}.

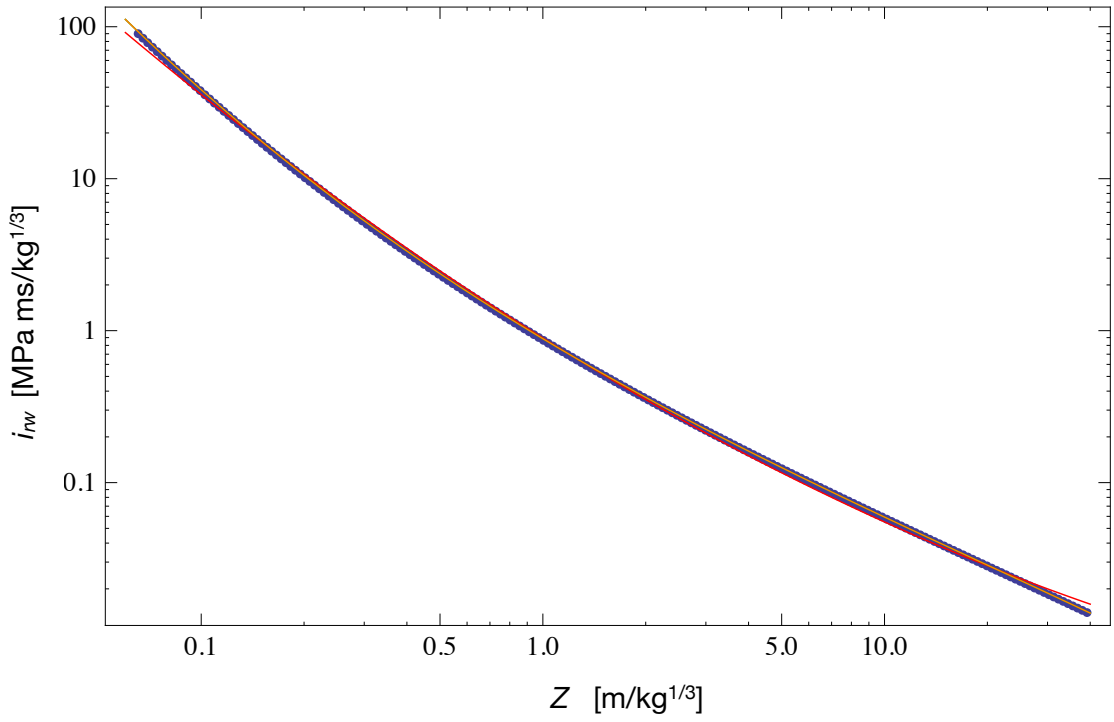

Figure 9: Comparison of experimental and fitted values of i_{rw}.

Table 2: Coefficients for the fitting functions of Swisdak (10), from [Swisdak, 1994]. ΔZ: range of validity in terms of the scaled distance (1) [m/kg$^{1/3}$].

ΔZ	k_0	k_1	k_2	k_3	k_4	k_5	k_6
			P_{so} [kPa]				
0.2 ÷ 2.9	7.2106	-2.1069	-0.3229	0.1117	0.0685		
2.9 ÷ 23.8	7.5938	-3.0523	0.40977	0.0261	-0.01267		
23.8 ÷ 198.5	6.0536	-1.4066					
			P_{ro} [kPa]				
0.06 ÷ 2	9.006	-2.6893	-0.6295	0.1011	0.29255	0.13505	0.019736
2 ÷ 40	8.8396	-1.733	-2.64	2.293	-0.8232	0.14247	-0.0099
			i_{sw} [kPa ms/kg$^{1/3}$]				
0.2 ÷ 0.96	5.522	1.117	0.6	-0.292	-0.087		
0.96 ÷ 2.38	5.465	-0.308	-1.464	1.362	-0.432		
2.38 ÷ 33.7	5.2749	-0.4677	-0.2499	0.0588	-0.00554		
33.7 ÷ 158.7	5.9825	-1.062					
			i_{rw} [kPa ms/kg$^{1/3}$]				
0.06 ÷ 40	6.7853	-1.3466	0.101	-0.01123			
			t_{Aw} [ms/kg$^{1/3}$]				
0.06 ÷ 1.5	-0.7604	1.8058	0.1257	-0.0437	-0.0310	-0.00669	
1.5 ÷ 40	-0.7137	1.5732	0.5561	-0.4213	0.1054	-0.00929	
			t_{ow} [ms/kg$^{1/3}$]				
0.2 ÷ 1.02	0.5426	3.2299	-1.5931	-5.9667	-4.0815	-0.9149	
1.02 ÷ 2.8	0.5440	2.7082	-9.7354	14.3425	-9.7791	2.8535	
2.8 ÷ 40	-2.4608	7.1639	-5.6215	2.2711	-0.44994	0.03486	

The comparison of eq. (12) with eq. (10) and the experimental data is shown in Fig. 11.

From the diagrams presented in Figs. 6 to 11, it appears clearly that, unlike eqs. (9) and (10), eq. (11) fits rather well, by a unique set of coefficients, the experimental data over the whole interval of Z, i.e. from the near field to the far field. The fitting of the experimental data obtained by eq. (10) is always very precise, but the analytical representations that we propose, represent with a high degree of accuracy the experimental data with the advantage of giving, in all the cases presented here, a unique analytical expression of each physical parameter over the whole range of variation of Z. We hence use the above analytical expression for the method for the computation of P_r that we propose in Sect. 5.2.

4.2 Influence of the type of explosive

The experimental data and formulae for the blasts are always referred to TNT, used as reference explosive. To assess the effects of a blast produced by another explosive, an equivalent weight W of TNT is computed according to the following formula, that links the weight W_e of a chosen explosive to W using the ratio of the heat produced during detonation, [Karlos and Solomos, 2013]:

$$W = W_e \frac{H_e}{H_{TNT}}, \tag{17}$$

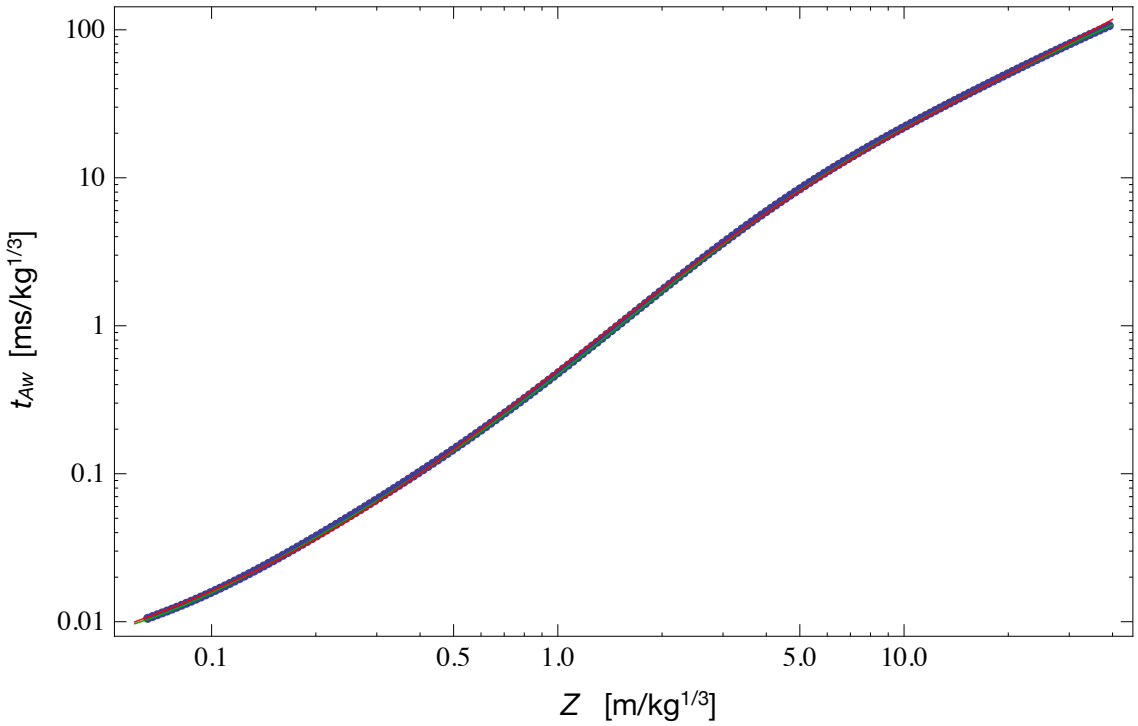

Figure 10: Comparison of experimental and fitted values of t_{Aw}.

where H_e is the heat of detonation of the explosive and H_{TNT} is that of TNT. The values of the heat of detonation of some explosives are given in Tab. 3.

Table 3: Heat of detonation of different explosives (from [Karlos and Solomos, 2013]).

Type of explosive	**Heat of detonation** [MJ/kg]
TNT	$4.10 \div 4.55$
C4	5.86
RDX	$5.13 \div 6.19$
PETN	6.69
Pentolite 50/50	5.86
Nitroglycerin	6.30
Nitromethane	6.40
Nitrocellulose	10.60

5 A procedure for computing P_r using TM5-1300

5.1 Influence of the direction

The values of the incident, P_{so}, and reflected, P_{ro}, pressures and impulses, i_{sw} and i_{rw} respectively, are intended for a normal shock, i.e. when the vector $q - o$ is orthogonal to the impinged surface in q. In such a case, the reflected pressure takes its maximum local

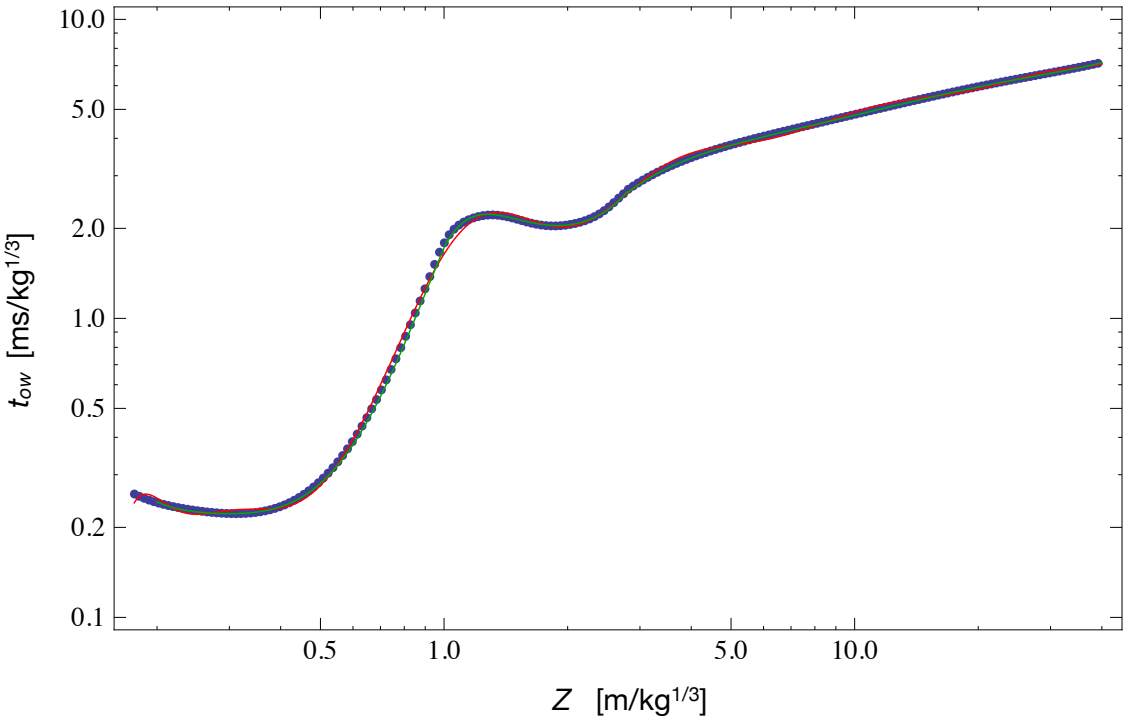

Figure 11: Comparison of experimental and fitted values of t_{ow}.

value, that decreases when the shock is not orthogonal, i.e. when the vector $q - o$ forms an angle $\alpha > 0$ with the inward normal to the impinged surface.

The effect of the lack of orthogonality in the shock is taken into account introducing the *reflection coefficient* $c_{r\alpha}$, defined as

$$c_{r\alpha} = \frac{P_{r\alpha}}{P_{so}}, \tag{18}$$

where $P_{r\alpha}$ is the peak of the reflected pressure in q for a surface inclined of the angle α onto the direction of $q - o$. It is worth noticing that the reflection coefficient is defined as the ratio of the reflected inclined pressure $P_{r\alpha}$ with the incident pressure P_{so}, not P_{ro}.

The value of $c_{r\alpha}$ has been evaluated experimentally, and the results are shown in Fig. 12; this figure has been obtained from the parametrized curves given in [Karlos and Solomos, 2013]. To remark that $c_{r\alpha}$ depends not only upon α, but also upon P_{so}.

In Fig. 13 we show also the interpolation of the empirical values of $i_{r\alpha w}$, still obtained from [Karlos and Solomos, 2013].

Looking at Fig. 12, one can see that $c_{r\alpha}$ is not a decreasing function of α, as it could be expected. Actually, for $\alpha >\sim 40°$, $c_{r\alpha}$ increases reaching a maximum and then it decreases again. This fact is attributed to the creation of the Mach stem cited above. For small values of P_{so} the behavior is more complicated, but this presumably could be the effect of uncertainties and imperfections in the experimental data.

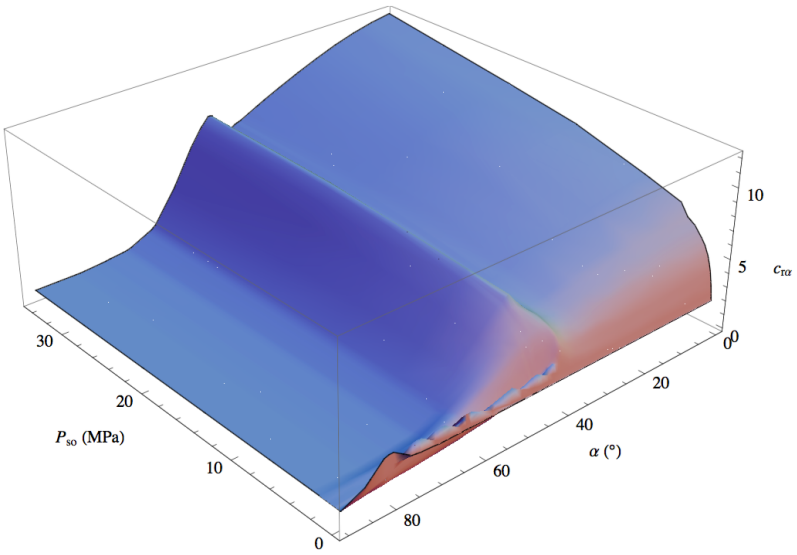

Figure 12: Surface representing $c_{r\alpha}(\alpha, P_{so})$.

5.2 P_r calculation

We detail in the following the sequence of the calculations to obtain, for a given blast, the time history of the reflected pressure $P_r(q,t)$ at the time t on a point q of a surface placed at a distance R from the detonation point o and whose inward normal forms an angle α with the vector $q-o$.

We make the following assumptions: i) the blast occurs at point o and is produced by a mass W_e of a given explosive; ii) the blast is hemispherical; iii) the time rate decrease is of the same type for P_s and P_r and it is ruled by the Friedlander's equation; iv) the calculation of the time history of P_s and P_r, as well as the impulse, is made pointwise; v) only the positive duration phase is considered (this assumption, usually done, is justified because of the much larger values of the positive pressures in comparison with the negative ones); finally, vi) reflected waves and dynamic pressure are ignored.

Then, the calculation sequence is the following one:

- a time duration t_{max} is fixed;
- t_{max} is subdivided into time intervals dt;
- the impinged surface is discretized into regular patches, whose centroids are points q;
- the equivalent mass of TNT W is calculated using eq. (17);
- then, for each point q we calculate:
  - the distance from the blast point: $R = ||q-o||$;
  - the inward normal $\mathbf{n}$ to the wall;
  - the angle α between $q-o$ and $\mathbf{n}$:

$$\cos\alpha = \frac{q-o}{R} \cdot \mathbf{n}; \tag{19}$$

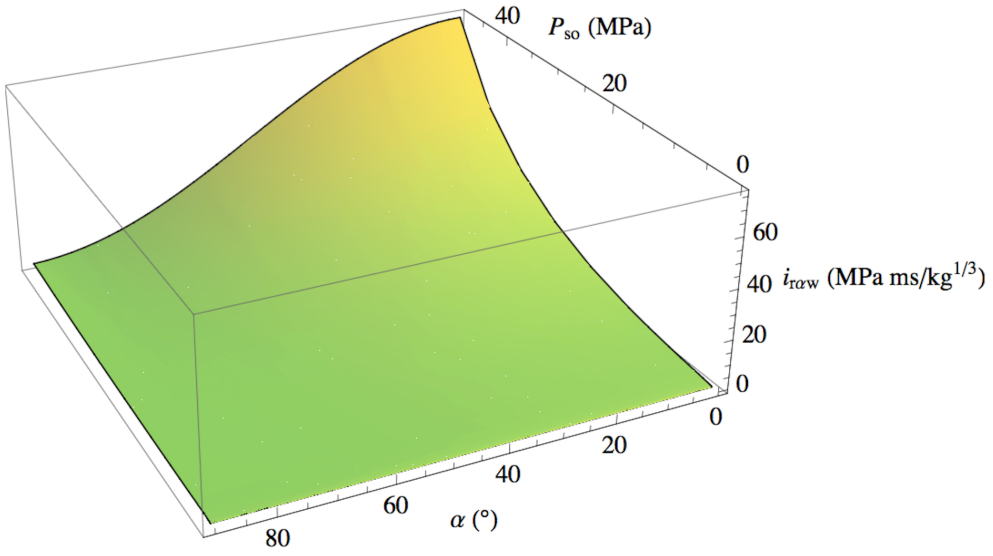

Figure 13: Surface representing $i_{r\alpha w}(\alpha, P_{so})$.

– the scaled distance Z, eq. (1);

– the normal incident pressure peak P_{so} using the fitted curve of Kingery-Bulmash for hemispherical blasts, eq. (11), Fig. 6;

– the normal reflected pressure peak P_{ro} using the fitted curve of Kingery-Bulmash for hemispherical blasts, eq. (12), Fig. 7;

– the ratio

$$c = \frac{P_{ro}}{P_{so}}; \tag{20}$$

– the angular coefficient $c_{r\alpha}$, eq. (18), by a linear interpolation of the experimental data represented by the surface in Fig. 12;

– the ratio

$$c_{r0} = \frac{P_{r0}}{P_{so}}, \tag{21}$$

i.e. $P_{r\alpha}$ for $\alpha = 0°$, still linearly interpolating the data of the surface in Fig. 12;

– the corrected value of $P_{r\alpha}$ as

$$P_{r\alpha} = c\frac{c_{r\alpha}}{c_{r0}}P_{so} = \frac{c_{r\alpha}}{c_{r0}}P_{ro}; \tag{22}$$

this correction is done to adapt the data of the interpolating surface in Fig. 12 to those of the Kingery-Bulmash fitted curves, Fig. 5, more conservative;

– the reduction coefficient

$$c_{red} = \frac{P_{r\alpha}}{P_{ro}} = \frac{c_{r\alpha}}{c_{r0}}; \tag{23}$$

– the positive normal scaled reflected impulse i_{rw} using the fitted curve of Kingery-Bulmash for hemispherical blasts, eq. (14), Fig. 9;

– the effective angular reflected impulse $i_{r\alpha}$ as

$$i_{r\alpha} = c_{red}\ i_{rw}\ W^{\frac{1}{3}}; \tag{24}$$

the value of $i_{r\alpha}$ is voluntarily *not* calculated interpolating the surface of experimental data, Fig. 13, like for $c_{r\alpha}$, because it has been observed, numerically, that the procedure described here is conservative;

– the scaled arrival time t_{Aw} using the fitted curve of Kingery-Bulmash for hemispherical blasts, eq. (15), Fig. 10;

– the arrival time t_A as

$$t_A = t_{Aw} W^{\frac{1}{3}}; \tag{25}$$

– the scaled positive duration time t_{ow} using the fitted curve of Kingery-Bulmash for hemispherical blasts, eq. (16), Fig. 11;

– the positive duration time t_o as

$$t_o = t_{ow} W^{\frac{1}{3}}; \tag{26}$$

– the fictitious positive duration time t_{rf}, eq. (4), as

$$t_{rf} = 2\frac{i_{r\alpha}}{P_{r\alpha}}; \tag{27}$$

– check on t_o: if $t_o < t_{rf}$ then put $t_o = 1.1\ t_{rf}$; this is done to avoid pathological situations, due to the fact that the Kingery-Bulmash curve for t_o does not cover low ranges of Z, see Figs. 5 and 11;

– solve numerically the equation

$$\frac{b - 1 + e^{-b}}{b^2} P_{r\alpha}\ t_o = i_{r\alpha} \tag{28}$$

to determine the coefficient b of the Friedlander's equation.

- the time history of the pressure wave can now be calculated:
  – $t = n\ dt$;
  – $\forall q$:
    * if $t < t_A$ or $t > t_A + t_o$ then $P_r(q,t) = 0$;
    * else, use the Friedlander equation (5) with $P_{r\alpha}$ in place of P_{so} to evaluate $P_r(q,t)$;
  – iterate on t until $t > t_{max}$.

This sequence has been implemented in a program for the formal code *Mathematica* and applied to the case study presented in Sec. 7.

6 The CONWEP model

CONWEP is the acronym of CONventional Weapons Effects Programme, a study made by USACE, [USACE, 1986], for the simulation of the effects of a blast produced by conventional, i.e. not nuclear, explosives. The report [USACE, 1986] uses in many parts the same experimental results shown above, but not completely; in particular, a noticeable difference is the way in which the reflected pressure is calculated; in place of using the data represented in Fig. 13, and integrating the effect of the Mach stem, CONWEP makes use of the following law, using circular functions:

$$P_{r\alpha} = \begin{cases} P_{so}(1 + \cos\alpha - 2\cos^2\alpha) + P_{ro}\cos^2\alpha & \text{if } \cos\alpha \geq 0, \\ P_{so} \quad \text{if } \cos\alpha < 0. \end{cases} \tag{29}$$

The algorithm CONWEP is today implemented in different finite elements commercial codes, e.g. in *LS-DYNA*, *AUTODYN* or *ABAQUS*. In particular, in *ABAQUS*, the code we used for numerical simulations with CONWEP, the following assumptions are made: i) for each point q of the impinged walls, $P_{r\alpha}$ is calculated according to eq. (29); ii) reflected waves are ignored; iii) the dynamic pressure is neglected; iv) the negative phase is taken into account; v) hemispherical blasts can be modeled.

The assumptions made by CONWEP are similar to those introduced in Sec. 5.2, except for the calculation of $P_{r\alpha}$ and the fact that in CONWEP the negative phase is considered too. This is why a comparison of the two methods is interesting, see Sec. 7.

A final, important remark: neglecting the reflected waves and the dynamic pressure means that there is no difference between internal and external blasts: the only geometric parameters that matter are R and α, regardless the surrounding geometry. For numerical simulations, this is interesting and important because it allows modeling only a part of the building, the closest one to the detonation point, and reasonably neglecting the effects, at least in terms of applied pressures, of more distant parts. Therefore, only a part of the building can be modeled, reducing in this way the calculation cost, but of course reducing in the same time the degree of accuracy compared to more physical approaches, like the JWL, which are able to cover all the aspects of the blast wave.

7 Comparison of the models on a case study

Even though CONWEP and JWL models are implemented in some commercial finite element codes, this is apparently not the case for the model TM5-1300. This is probably due to the fact that it is much easier to implement the dependence on the direction described by eq. (29) than the more accurate of TM5-1300, described in Fig. 12.

As said above, in the case of large buildings, like monuments, to make a complete nonlinear fluid-solid simulation using the model JWL is computationally expensive and unnecessary from an engineering point of view. This is why CONWEP is generally preferred, but its accuracy has to be assessed. The following comparison is hence made with the objective of evaluating the response of the model CONWEP, in comparison with both JWL and TM5-1300.

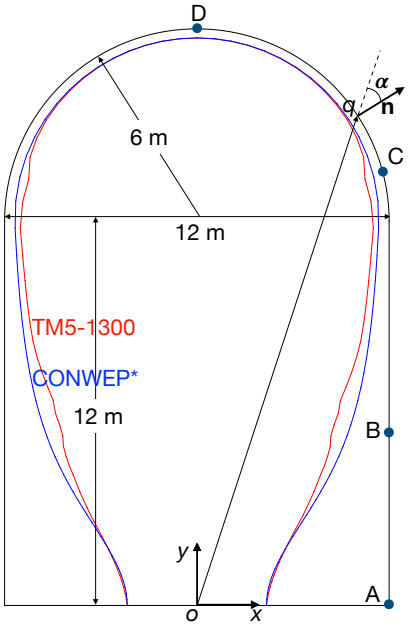

Figure 14: Case study: layout and $P_{r\alpha}$ distribution for the model TM5-1300 and CONWEP*.

To evaluate the differences in the prediction of the blast parameters, and namely of the reflected pressure between the three models, we consider an explosion in the interior of a building covered by a barrel vault, see Fig. 14. This is intended to simulate the typical structure of a monumental building, like a church or a palace gallery and so on. The dimensions used in this case are: width: 12 m, height of the walls: 12 m, radius of the vault: 6 m, total height: 18 m.

The explosive charge is composed by $W = 20$ kg of TNT, and detonates at the instant $t = 0$ at point $o = (0, 0)$. The problem is treated as a planar one, exception made for the JWL model, where a 3D approach is used.

The evaluation of $P_{r\alpha}$ is done in four different ways: in the first one, we use the JWL model; the results are indicated as JWL. Then, we have used the data of TM5-1300 and following modifications, as integrated into [Karlos and Solomos, 2013], and according to the calculation sequence presented in Sec. 5.2; the results are indicated as TM5-1300. The third way, is the use of the data of TM5-1300 and following modifications, as integrated into [Karlos and Solomos, 2013], but evaluating the pressure $P_{r\alpha}$ according to eq. (29); the results are indicated as CONWEP*. Finally, we have applied the model CONWEP as implemented in *ABAQUS* to the above structure; the results are indicated as CONWEP. The results TM5-1300 and CONWEP* have been obtained using the program we have done in *Mathematica*.

7.1 The results from JWL

The analyses with the JWL model are run with *AUTODYN Hydrocode*, a code allowing good facilities in modeling the set of explosive, air domain and structure, where the equations of mass, momentum and energy conservation for inviscid flows are coupled with the dynamic equations of solid continua. A *Coupled Eulerian-Lagrangian* (CEL) method is used: explosive and surrounding air, as fluids, are modeled with an Eulerian frame, while solid walls are identified in a Lagrangian reference.

The 3D geometrical model, taking advantage of symmetries, consists of a quarter of the entire domain. A volume having the transversal section like in Fig. 14 and a depth of 2 m is hence discretized. Ground and planes of symmetry are modeled as *reflecting planes* to prevent flow of material through them. The ending transversal surfaces are modeled as *transmitting planes*, i.e. boundary surfaces whereupon the gradients of velocity and stress are put to zero. This approach is used to simulate a far field solution at the boundary, it is only exact for outflow velocities higher than the speed of sound and is an approximation for lower velocities.

A preliminary study of the solution sensitivity to the cells size has been made studying the peak of the reflected pressure at point A of Fig. 14 for five different meshes. For each one of them, the dimensions of the volume elements discretizing the explosive charge and of the surface elements modeling the explosive-air and air-solid interfaces are decreased each time by a factor 1.5 starting from the coarsest mesh.

In Tab. 4 and in Fig. 15 we show the relative percent error, computed with respect to the finest discretization; it is apparent that it remains very small in all the cases. Attention needs to be paid when dealing with a CEL approach: more precisely, an almost equal size of the Eulerian and Lagrangian elements and an average grid size smaller than the thickness of the solid walls must be guaranteed. The simulations have been made with the mesh M2.

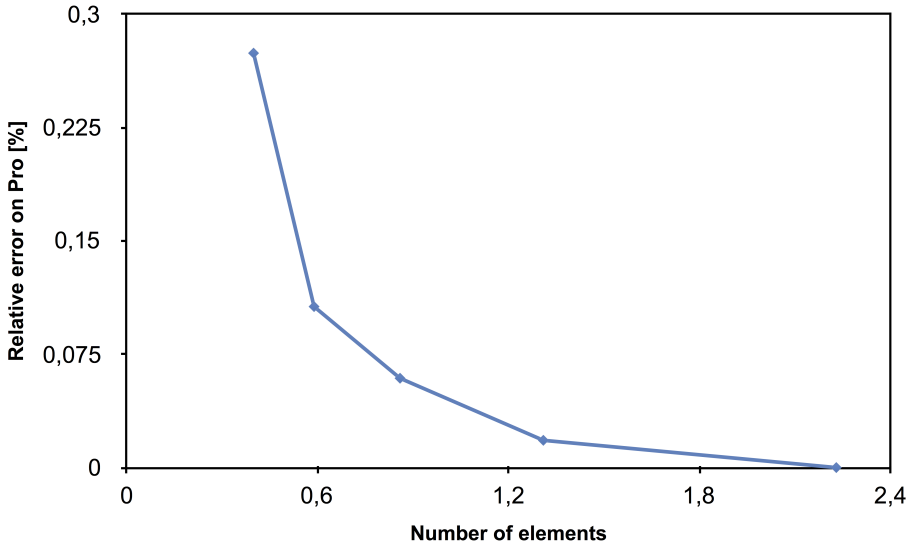

Figure 15: Convergence study for different meshes.

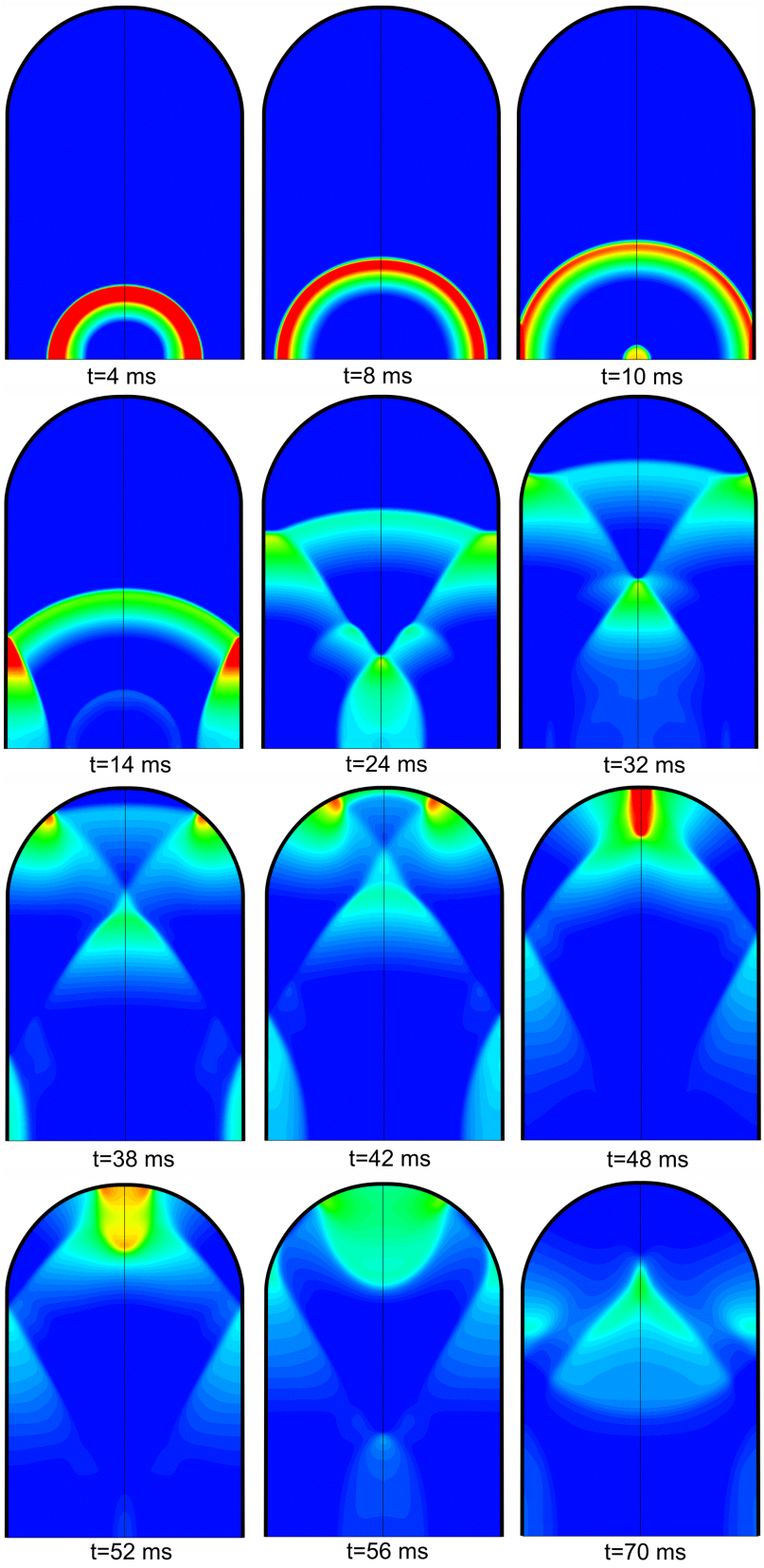

Figure 16: Evolution of the shock-wave as predicted by JWL; the color scale represents the overpressure and runs from blue for the minimum value, 0 kPa, to red for the maximum one, 300 kPa

Table 4: Convergence study for different meshes.

Meshes	$\mathbf{M_1}$	$\mathbf{M_2}$	$\mathbf{M_3}$	$\mathbf{M_4}$	$\mathbf{M_5}$
Number of elements [10^6]	2.23	1.31	0.86	0.59	0.4
Relative error on P_{ro} at point A [%]	0.	0.018	0.059	0.106	0.274

The results of the numerical simulation are presented in Fig. 16. It is apparent the formation not only of the principal, hemispheric shock-wave, but also of the reflected ones, that produce the Mach stem, well visible in the photogram at $t = 14$ ms, at the bottom of the waves reflected by the vertical walls. At $t \sim 48$ ms, the incident and reflected waves focus just at the top of the vault, giving rise to a very high localized pressure. Then, the reflected waves propagate downwards and upwards and decrease in intensity. Though not well visible in the figures, also the dynamic pressure is taken into account in this analysis.

The focusing of waves in the vault is not a surprising result and it is very similar to what observed by Rayleigh for acoustic waves in the study of the *whispering galleries*, [J. W. Strutton - Lord Rayleigh, 1910, 1914]: due to its geometry, the vault behaves like a concave (i.e. converging) mirror for the shock waves, which has the tendency to collect the blast energy. As far as it concerns blasts, we can hence say that barrel vaults and domes have a dissatisfactory behavior.

What is clear, is the true complexity of the pressure dynamics, which cannot be predicted in advance and, most important, that is strongly depending upon the geometry and dimensions of the structure. Namely, the focusing of the shock waves described hereon takes place just because of the geometry of the vault and of its dimensions. To this purpose, we have also performed a simulation where the lowest part of the vertical walls, for a height of 7 m, are replaced by transmitting planes, to simulate the presence of openings, like in the case of an aisle. In such simulation, the focus, at the key of the vault, of the reflected waves, gives a sensibly smaller peak of the reflected pressure, reduced by a factor 2.72 with respect to that calculated in the above simulation, see Fig. 17, passing from 0.299 to 0.109 MPa.

It is not possible to recover such a complete description of the pressure history everywhere in the fluid domain, and on the walls, using the other empirical models. Therefore, it is interesting, for the comparison, to have the time-history of the pressure at a given point of the solid boundary. To this purpose, we give in Fig. 18 the diagram of the time variation of the reflected pressure P_r at four points of the boundary, indicated in Fig. 14 as points A, at the base of the vertical vault ($Z = 2.21$ m/kg$^{1/3}$), B, at 5.63 m from the base of the vertical wall ($Z = 3.03$ m/kg$^{1/3}$), C, at the springing of the vault ($Z = 5.40$ m/kg$^{1/3}$), and D, the key of the vault ($Z = 6.63$ m/kg$^{1/3}$).

It is apparent that the decay phase is not exactly as predicted by the Friedlander's law, and this because of the reflected waves, clearly visible on each diagram as secondary peaks of the curve. It is interesting to notice that the successive peaks are not necessarily decreasing, which confirms the complexity of the interactions and dynamics of the reflected waves.

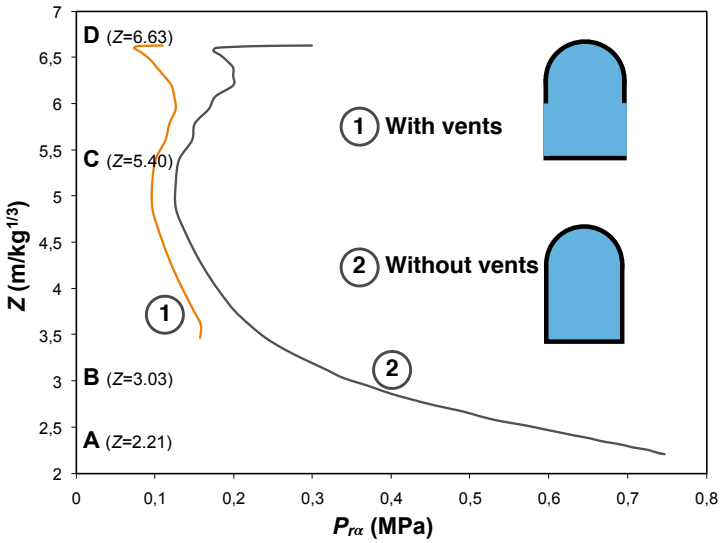

Figure 17: Comparison of $P_{r\alpha}$ as obtained by JWL for the two cases of vertical openings until the height of 7 m (curve 1) and of complete vertical walls (curve 2).

Table 5: Simulation results for models TM5-1300 ($P_{r\alpha}1$) and CONWEP* ($P_{r\alpha}2$).

#	x [m]	y [m]	R [m]	Z $\left[\mathrm{m/kg^{1/3}}\right]$	α [°]	φ [°]	$P_{r\alpha}1$ [MPa]	$P_{r\alpha}2$ [MPa]	t_A [ms]	t_o [ms]	$t_A + t_o$ [ms]	b
1.	6.	0.	6.	2.21042	0.	90.	0.765485	0.765485	5.80175	5.70184	11.5036	3.88204
2.	6.	0.188558	6.00296	2.21151	1.8	90.	0.760041	0.76395	5.8068	5.70346	11.5103	3.87904
3.	6.	0.377488	6.01186	2.21479	3.6	90.	0.752468	0.759364	5.82198	5.70837	11.5304	3.87009
4.	6.	0.567167	6.02675	2.22027	5.4	90.	0.742913	0.751779	5.84741	5.71668	11.5641	3.85531
5.	6.	0.757976	6.04769	2.22799	7.2	90.	0.731543	0.741284	5.88325	5.72862	11.6119	3.83489
6.	6.	0.950307	6.07479	2.23797	9.	90.	0.71823	0.728	5.92975	5.74448	11.6742	3.80909
7.	6.	1.14456	6.10819	2.25028	10.8	90.	0.703064	0.712079	5.98724	5.76463	11.7519	3.77826
8.	6.	1.34116	6.14807	2.26497	12.6	90.	0.686672	0.693701	6.05612	5.78955	11.8457	3.74281
9.	6.	1.54054	6.19462	2.28212	14.4	90.	0.668886	0.673071	6.13689	5.81981	11.9567	3.70319
10.	6.	1.74316	6.24809	2.30182	16.2	90.	0.64965	0.650416	6.23013	5.85607	12.0862	3.65994
11.	6.	1.94952	6.30877	2.32417	18.	90.	0.629087	0.62598	6.33654	5.89908	12.2356	3.61361
12.	6.	2.16013	6.377	2.34931	19.8	90.	0.607325	0.60002	6.45693	5.94972	12.4067	3.5648
13.	6.	2.37557	6.45316	2.37737	21.6	90.	0.584501	0.572801	6.59223	6.00893	12.6012	3.51413
14.	6.	2.59643	6.5377	2.40851	23.4	90.	0.560758	0.544596	6.74353	6.07776	12.8213	3.46222
15.	6.	2.82339	6.6311	2.44292	25.2	90.	0.536604	0.515674	6.91207	6.15734	13.0694	3.40968
16.	6.	3.05715	6.73396	2.48081	27.	90.	0.514591	0.486303	7.09928	6.24889	13.3482	3.35705
17.	6.	3.29853	6.84692	2.52243	28.8	90.	0.491878	0.456741	7.3068	6.35366	13.6605	3.30483
18.	6.	3.54839	6.97073	2.56804	30.6	90.	0.469527	0.427236	7.53652	6.47291	14.0094	3.2534
19.	6.	3.80772	7.10624	2.61796	32.4	90.	0.448879	0.398019	7.79061	6.60789	14.3985	3.20301
20.	6.	4.0776	7.25443	2.67256	34.2	90.	0.427992	0.369304	8.07157	6.75974	14.8313	3.1537
21.	6.	4.35926	7.41641	2.73223	36.	90.	0.403807	0.341285	8.38228	6.92942	15.3117	3.10531
22.	6.	4.65408	7.59345	2.79745	37.8	90.	0.384418	0.314131	8.72609	7.11756	15.8437	3.05738
23.	6.	4.96363	7.78702	2.86876	39.6	90.	0.367394	0.287992	9.10688	7.32437	16.4312	3.00913
24.	6.	5.28971	7.99882	2.94679	41.4	90.	0.363427	0.262988	9.52915	7.54941	17.0786	2.95941
25.	6.	5.63438	8.23081	3.03226	43.2	90.	0.343876	0.239219	9.99818	7.79141	17.7896	2.90667
26.	6.	6.	8.48528	3.126	45.	90.	0.317226	0.216758	10.5202	8.04807	18.5683	2.84899
27.	6.	6.38935	8.76492	3.22902	46.8	90.	0.304107	0.195655	11.1025	8.31585	19.4183	2.78408
28.	6.	6.80566	9.07288	3.34248	48.6	90.	0.270092	0.175939	11.7538	8.58988	20.3436	2.70941
29.	6.	7.25275	9.41289	3.46774	50.4	90.	0.2356	0.157617	12.4844	8.86397	21.3483	2.62239
30.	6.	7.73515	9.78941	3.60645	52.2	90.	0.203598	0.140679	13.3068	9.13083	22.4376	2.5206
31.	6.	8.25829	10.2078	3.76059	54.	90.	0.177162	0.125096	14.2361	9.38266	23.6187	2.40217
32.	6.	8.82873	10.6746	3.93255	55.8	90.	0.158073	0.110828	15.2906	9.61206	24.9026	2.26615
33.	6.	9.45449	11.1976	4.12525	57.6	90.	0.141759	0.0978226	16.4929	9.81332	26.3062	2.11303
34.	6.	10.1454	11.7869	4.34232	59.4	90.	0.127267	0.0860183	17.8711	9.98409	27.8552	1.94507
35.	6.	10.914	12.4545	4.58828	61.2	90.	0.112877	0.0753469	19.4605	10.127	29.5875	1.76667
36.	6.	11.7757	13.2161	4.86887	63.	90.	0.0983451	0.0657355	21.3057	10.2512	31.557	1.58446
37.	5.96239	12.6707	14.0035	5.15893	58.3816	83.5816	0.106085	0.0626654	23.2452	10.3613	33.6065	1.42342
38.	5.82149	13.4527	14.6582	5.40014	52.5888	75.9888	0.11852	0.0616353	24.88	10.4518	35.3318	1.31115
39.	5.60197	14.1489	15.2176	5.6062	47.4129	69.0129	0.0852345	0.0607484	26.2908	10.5337	36.8245	1.23022
40.	5.31949	14.7754	15.7038	5.78534	42.6467	62.4467	0.0750139	0.0599822	27.5269	10.6104	38.1374	1.17038
41.	4.98432	15.3401	16.1296	5.94219	38.1727	56.1727	0.0684349	0.0593205	28.6161	10.6825	39.2987	1.12546
42.	4.60409	15.8474	16.5026	6.07963	33.9164	50.1164	0.0656936	0.0587507	29.5755	10.7497	40.3252	1.09142
43.	4.185	16.2995	16.8282	6.19956	29.8268	44.2268	0.0634732	0.0582626	30.4163	10.8113	41.2276	1.0655
44.	3.7324	16.6978	17.1098	6.30332	25.8672	38.4672	0.0616696	0.0578481	31.1463	10.8669	42.0131	1.04573
45.	3.2511	17.0429	17.3502	6.39186	22.0096	32.8096	0.0602101	0.0575007	31.7709	10.9159	42.6868	1.0307
46.	2.74559	17.335	17.551	6.46586	18.2322	27.2322	0.0590426	0.057215	32.2942	10.9579	43.2522	1.01937
47.	2.22013	17.5741	17.7138	6.52583	14.517	21.717	0.0581296	0.0569866	32.7191	10.9927	43.7119	1.01097
48.	1.67885	17.7603	17.8395	6.57213	10.8487	16.2487	0.057444	0.0568122	33.0477	11.02	44.0677	1.00494
49.	1.12576	17.8934	17.9288	6.60503	7.21431	10.8143	0.0569668	0.0566894	33.2814	11.0396	44.321	1.00089
50.	0.564835	17.9734	17.9822	6.62471	3.60178	5.40178	0.0566853	0.0566164	33.4213	11.0514	44.4727	0.998567
51.	0.	18.	18.	6.63126	0.	0.	0.0565922	0.0565922	33.4678	11.0553	44.5232	0.997807

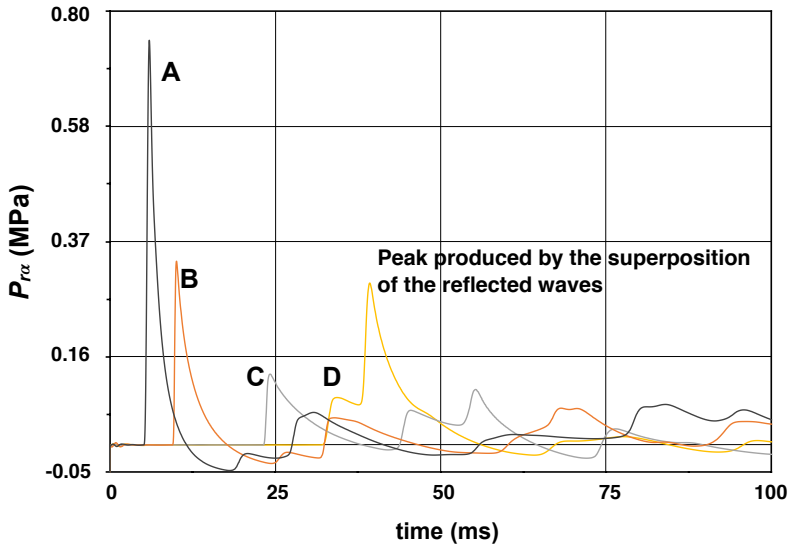

Figure 18: Time variation of $P_{r\alpha}$ at four points of the solid boundary, by JWL.

7.2 The results from TM5-1300 and CONWEP*

The spatial distributions of the maximum value of $P_{r\alpha}$ as given by TM5-1300 and CONWEP*, and calculated as specified above and in Sect. 5.2, are shown in Fig. 14. Such distributions are similar, though some differences exist: first of all, CONWEP* gives maximum values of $P_{r\alpha}$ that are almost always less or equal of those given by TM5-1300. Then, the greatest differences appear for $0° < \alpha < 90°$; this can be explained by the fact that the angular variation taken by CONWEP does not take into account for the formation of the Mach stem.

Such occurrence happens for $\alpha \simeq 40°$ and it is clearly indicated by the local increase of $P_{r\alpha}$ in the diagram of TM5-1300, that shows two humps: at midway of the vertical wall and at the springing of the vault where $\alpha \simeq 40°$ in both the cases; this fact can be of a great importance for vaulted structures, because an increase of $P_{r\alpha}$ in the zone between 0° and 30° can be very dangerous for the stability of the vault, that normally has on its back a filling with a material like rubble or gravel in order to improve the structural stability of the structure.

The numerical data of the simulations TM5-1300 and CONWEP* are shown in Tab. 5; φ is the angle formed by the normal $\mathbf{n}$ with the axis y, while b is the coefficient appearing in the Friedlander's law, eq. (5).

Observing the results concerning $P_{r\alpha}$ and t_o, we see clearly that the peak of the shock wave decreases with the distance R, passing from a maximum of 0.736 MPa for $R = 6$ m, to a minimum of 0.063 MPa for $R = 18$ m, while its time duration increases, passing from 7.2 ms to 11 ms.

In Fig. 19 we show the same curves of Fig. 18 but now obtained with the models TM5-1300, red curves, and CONWEP*, green curves. The red and green curves are distinct only for $\alpha \neq 90°$, for the way the values of CONWEP* are calculated.

Table 6: Simulation results for the CONWEP model.

#	x [m]	y [m]	R [m]	Z $\left[\mathrm{m/kg^{1/3}}\right]$	α [°]	φ [°]	$P_{r\alpha}$ [MPa]	t_A [MPa]	t_o [ms]	$t_A + t_o$ [ms]
1.	6.	.001	6.	2.21042	.0096	90.	.771063	5.5634	5.7978	11.3612
2.	6.	.003	6.	2.21042	.0287	90.	.732472	5.6309	5.7303	11.3612
3.	6.	.005	6.	2.21042	.0478	90.	.740335	5.3609	5.7303	11.3612
4.	6.	.007	6.	2.21042	.0669	90.	.672189	5.7658	5.6628	11.4286
5.	6.	.504	6.02113	2.21820	4.8040	90.	.686422	5.7658	5.7975	11.5633
6.	6.	1.1	6.1	2.24726	10.3941	90	.703576	5.7658	5.7975	11.5633
7.	6.	1.3	6.13922	2.26171	12.2313	90.	.68598	5.8333	5.7974	11.6307
8.	6.	1.5	6.18466	2.27845	14.0434	90.	.604788	6.0357	5.7297	11.7654
9.	6.	1.7	6.23618	2.29743	15.8272	90.	.628755	6.0357	5.8645	11.9002
10.	6.	1.9	6.29365	2.3186	17.5802	90.	.561932	6.2381	5.7969	12.0349
11.	6.	2.3	6.42573	2.36726	20.9841	90.	.588982	6.2381	5.999	12.237
12.	6.	2.7	6.57951	2.42391	24.24	90.	.533496	6.4404	5.9988	12.4392
13.	6.	2.9	6.66408	2.45507	25.8091	90.	.536047	6.5079	5.9986	12.5065
14.	6.	3.1	6.75352	2.48802	27.3378	90.	.515549	6.6428	6.0659	12.7086
15.	6.	3.3	6.84763	2.52269	28.8254	90.	.475994	6.8451	6.2004	13.0455
16.	6.	3.5	6.94622	2.55901	30.2718	90.	.442626	7.0474	6.2001	13.2475
17.	6.	3.7	7.04911	2.59692	31.6768	90.	.414128	7.2497	6.1999	13.4496
18.	6.	3.9	7.15612	2.63634	33.0406	90.	.389846	7.452	6.2671	13.7191
20.	6.	4.1	7.26705	2.6772	34.3635	90.	.369243	7.6543	6.4016	14.0559
21.	6.	4.3	7.38173	2.71945	35.646	90.	.351181	7.8565	6.6035	14.46
22.	6.	4.5	7.5	2.76302	36.8886	90.	.335817	8.0588	6.6707	14.7295
23.	6.	4.7	7.62168	2.80785	38.0921	90.	.322735	8.2611	6.8726	15.1336
24.	6.	4.9	7.74661	2.85388	39.2573	90.	.311071	8.4633	7.0744	15.5377
25.	6.	5.1	7.87464	2.90104	40.385	90.	.290647	8.7329	7.2089	15.9418
26.	6.	5.3	8.00562	2.9493	41.4763	90.	.273256	9.0026	7.2087	16.2112
27.	6.	5.5	8.13941	2.99858	42.532	90.	.266726	9.2048	7.4105	16.6153
28.	6.	5.7	8.27587	3.04886	43.5533	90.	.244744	9.5418	7.4777	17.0194
29.	6.	5.9	8.41487	3.10006	44.5411	90.	.233275	9.8113	7.5449	17.3562
30.	6.	6.1	8.55628	3.15216	45.4966	90.	.216588	10.1483	7.6119	17.7602
31.	6.	6.3	8.7	3.20511	46.4207	90.	.214245	10.3504	7.8139	18.1643
32.	6.	6.5	8.8459	3.25886	47.3146	90.	.194903	10.7548	7.8809	18.6357
33.	6.	6.7	8.99389	3.31338	48.1793	90.	.188719	11.0243	8.0155	19.0398
34.	6.	6.9	9.14385	3.36862	49.0158	90.	.178286	11.3612	8.0826	19.4438
35.	6.	7.1	9.2957	3.42456	49.8251	90.	.173488	11.6307	8.2172	19.8479
36.	6.	7.3	9.44934	3.48117	50.6083	90.	.160889	12.0349	8.217	20.2519
37.	6.	7.5	9.60469	3.53840	51.3662	90.	.157606	12.3044	8.3516	20.656
38.	6.	7.7	9.76166	3.59623	52.1	90.	.150868	12.6413	8.4187	21.06
39.	6.	7.9	9.92018	3.65463	52.8103	90.	.141494	13.0455	8.4859	21.5314
40.	6.	8.1	10.08018	3.71357	53.4983	90.	.133298	13.4496	8.5532	22.0028
41.	6.	8.3	10.24158	3.77303	54.1646	90.	.131731	13.7191	8.6877	22.4068
42.	6.	8.5	10.40433	3.83299	54.8102	90.	.124746	14, 1232	8.8223	22.9455
43.	6.	8.7	10.56835	3.89341	55.4358	90.	.121109	14.46	8.8895	23.3495
44.	6.	8.9	10.73359	3.95429	56.0422	90.	.115390	14.8642	8.8893	23.7535
45.	6.	9.1	10.9	4.01559	56.6302	90.	.107966	15.3357	8.8892	24.2249
46.	6.	9.3	11.06752	4.07731	57.2005	90.	.107626	15.6051	9.1585	24.7636
47.	6.	9.5	11.2361	4.13942	57.7536	90.	.103298	16.0092	9.2257	25.2349
48.	6.	9.7	11.4057	4.2019	58.2904	90.	.099298	16.4133	9.2256	25.6389
49.	6.	9.9	11.57627	4.26473	58.8114	90.	.095704	16.8174	9.2929	26.1103
50.	6.	10.1	11.74777	4.32791	59.3172	90.	.092426	17.2215	9.4275	26.649
51.	6.	10.3	11.92015	4.39142	59.8085	90.	.086272	17.7602	9.2928	27.053
52.	6.	10.5	12.09339	4.45524	60.2857	90.	.083664	18.1643	9.36	27.5243
53.	6.	10.7	12.26744	4.51936	60.7494	90.	.082638	18.501	9.562	28.063
54.	6.	10.9	12.44227	4.58377	61.2001	90.	.080329	18.9051	9.6292	28.5343
55.	6.	11.1	12.61784	4.64845	61.6382	90.	.075713	19.4438	9.5618	29.0056
56.	6.	11.3	12.79414	4.7134	62.0643	90.	.073825	19.8479	9.6964	29.5443
57.	6.	11.5	12.97112	4.7786	62.4789	90.	.072095	20.2519	9.7637	30.0156
58.	6.	11.7	13.14876	4.84405	62.8822	90.	.070498	20.656	9.8983	30.5543
59.	6.	11.9	13.32704	4.90972	63.2748	90.	.067946	21.1273	9.8983	31.0256
60.	5.99832	12.10025	13.5054	4.97543	63.6638	90.	.064633	21.6661	9.8981	31.5642
61.	5.99163	12.30062	13.68228	5.0406	62.1427	88.0809	.064329	22.0028	10.0328	32.0356
62.	5.95817	12.70015	14.02831	5.16807	59.1296	84.2299	.062510	22.9455	10.1	33.0455
64.	5.85816	12.79302	14.07051	5.38362	63.5136	88.0843	.062294	24.2249	10.2346	34.4595
65.	5.69932	13.8729	14.99799	5.52531	50.2785	72.5782	.062214	25.4369	10.5038	35.9407
66.	5.48322	14.43397	15.44038	5.68828	45.9365	66.7023	.061377	26.6490	10.5036	37.1526
67.	5.21205	14.97060	15.85195	5.83991	41.6396	60.7994	.059801	27.8610	10.5708	38.4318
66.	4.88854	15.47738	16.23105	5.97957	37.3838	54.8758	.060474	28.8036	10.8402	39.6438
67.	4.09793	16.38143	16.88621	6.22093	28.9900	42.9962	.059756	30.6216	10.9073	41.5289
68.	3.47738	16.88854	17.24282	6.35231	23.4836	35.0786	.059435	31.6316	11.1092	42.7408
69.	2.43397	17.48322	17.65183	6.50299	15.3680	23.2520	.058859	32.8435	11.1765	44.0200
70.	1.29302	17.85816	17.90491	6.59623	7.4347	11.5324	.058495	33.6515	11.3111	44.9626
71.	.50299	17.93144	17.93850	6.6086	1.53009	.0318	.059572	33.7188	11.4458	45.1646
72.	.001	17.99832	17.99832	6.63064	.00319	.0456	.058515	34.0555	11.3784	45.4339

7.3 The results from CONWEP

The same case study has finally been implemented in *ABAQUS* in order to make a comparison also with the results given by the model CONWEP. The comparison, as already said, will serve to understand the quality of the predictions given by CONWEP and to calibrate its use.

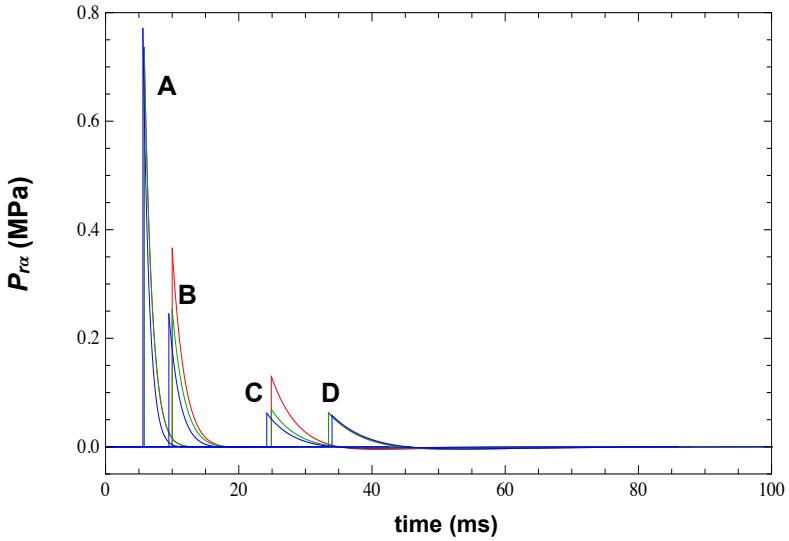

Figure 19: Time variation of $P_{r\alpha}$ at four points of the solid boundary, as predicted by TM5-1300 (red curves), CONWEP (blue curves) and CONWEP* (green curves).

The problem is still considered planar and the mesh consists of linear quadrilateral elements with an average size of 0.2 m and a thickness of 0.1 m.

The results obtained with this simulation are reported in Tab. 6, while the diagrams of the time variation of the reflected pressure P_r at the four points A, B, C and D of the boundary are still shown in Fig. 19.

7.4 Comparison

In order to compare the results of the above simulations, something must be mentioned about the results from JWL. On one hand, the multiple reflections of the shock-wave, visible in Fig. 16, completely alter the time variation of P_r after the positive phase, to such a point that in some cases the duration of the pure decaying phase can be really difficult to be determined. On the other hand, the multiple reflections add together and can considerably increase the value of P_r. Nevertheless, it is still possible, at least for a part of the boundary surface, to focus on just the characteristic elements of the positive phase, namely $P_{r\alpha}$, t_A and t_o. Such a comparison, of course, is possible only if the peak $P_{r\alpha}$ has not yet been affected by other reflected shock-waves and if a positive phase is still clearly distinguishable, which depends again on the reflected waves.

To assess the results, we have chosen to consider the relevant physical parameters of the blast: $P_{r\alpha}$, t_A and t_o. We have compared them as evaluated at the four points A, B, C and D of Fig. 14; these values are summarized in Tab. 7.

In Fig. 20 we show a comparison of the results for the values of $P_{r\alpha}$ obtained with JWL, TM5-1300, CONWEP* and CONWEP. The latter ones, as already pointed out, use the empirical data for computing P_r for $\alpha = 0$, but a different angular dependence from α, eq. (29).

It can be observed that the values given by CONWEP and the code *ABAQUS* are prac-

Table 7: Comparison of the characteristic parameters evaluated at points A, B, C and D of Fig. 14 as calculated by JWL, TM5-1300, CONWEP* and CONWEP; R_1 =*JWL/TM5-1300*, R_2 =*JWL/CONWEP*, R_3 =*TM5-1300/CONWEP*.

	JWL	**TM5-1300**	**CONWEP***	**CONWEP**	$\mathbf{R_1}$	$\mathbf{R_2}$	$\mathbf{R_3}$
			$\mathbf{P}_{r\alpha}$ [MPa]				
A	0.746	0.765	0.765	0.771	0.97	0.97	0.99
B	0.339	0.344	0.239	0.245	0.98	0.72	1.49
C	0.131	0.118	0.062	0.062	1.11	2.11	1.90
D	0.299	0.056	0.056	0.058	5.33	5.15	0.96
			$\mathbf{t_A}$ [ms]				
A	5.9	5.8	5.8	5.6	1.02	1.05	1.00
B	10.1	10.0	10.0	9.5	1.01	1.06	1.05
C	24.3	24.9	24.9	24.2	0.97	1.00	1.03
D	39.3	33.5	33.5	34.0	1.17	1.15	0.98
			$\mathbf{t_o}$ [ms]				
A	5.7	5.7	5.7	5.8	1.00	0.98	0.98
B	7.7	7.8	7.8	7.5	0.99	1.03	1.04
C	13.9	10.4	10.4	10.2	1.34	1.36	1.02
D	16.9	11.0	11.0	11.4	1.54	1.48	0.96

tically coincident with those calculated using the model CONWEP*, except some oscillations, to be imputed to the finite element approximation. Hence, on one side the computation of P_{ro} is practically the same for the three models, but what changes is the way the effect of the inclination α is taken into account. In particular, except the value $\alpha = 0$, where the three models give the same P_{ro}, for all the other values of α, CONWEP and CONWEP* underestimate the value of $P_{r\alpha}$ with respect to TM5-1300.

TM5-1300 and JWL give values that are comparable until point C; here, JWL diverges and gives values of $P_{r\alpha}$ that can be considerably greater. This is actually the effect of converging the reflected waves, that increases significantly the value of the overpressure. It is a local phenomenon, essentially depending upon the geometry and dimensions of the structure, as shown above. This same phenomenon is noticed also on the time variation of $P_{r\alpha}$ for point D in Fig. 18, where the peak due to the reflected waves is clearly visible.

It is worth noticing that, besides the convergence of the reflected waves starting from point C, JWL and TM5-1300 give not only comparable values of $P_{r\alpha}$, but also of its time variation. In Fig. 21 we show the time diagrams of JWL, reduced to the positive phases, presented together with those of TM5-1300. The curves are in a rather good agreement, apart from the peak on the curve of point D, due to reflected waves.

As far as it concerns the time durations, represented in Fig. 22, TM5-1300 and CONWEP* give, of course, the same values, while CONWEP underestimates slightly the durations for small values of Z. Nevertheless, these discrepancies are not significant. The diagrams in Figs. 20 and 22 explain the aforementioned slight differences, namely in the value of t_A, appearing in Fig. 19 between the curves obtained with CONWEP and those relative to TM5-1300 and CONWEP*.

For what concerns JWL, the curve of t_A is in a very good agreement with those of TM5-1300 and CONWEP until point C, where it diverges, once more due to wave reflection. The curve of $t_A + t_o$ has been obtained by interpolating the values estimated for points A, B, C and D for the duration t_o because, as mentioned above, it is not easy to determine the exact duration of the positive phase for all the points, due to the interaction of the reflected waves. Globally, the four models give values that are comparable, apart the zone of the wave reflections, where the values given by JWL diverge from those of the other models.

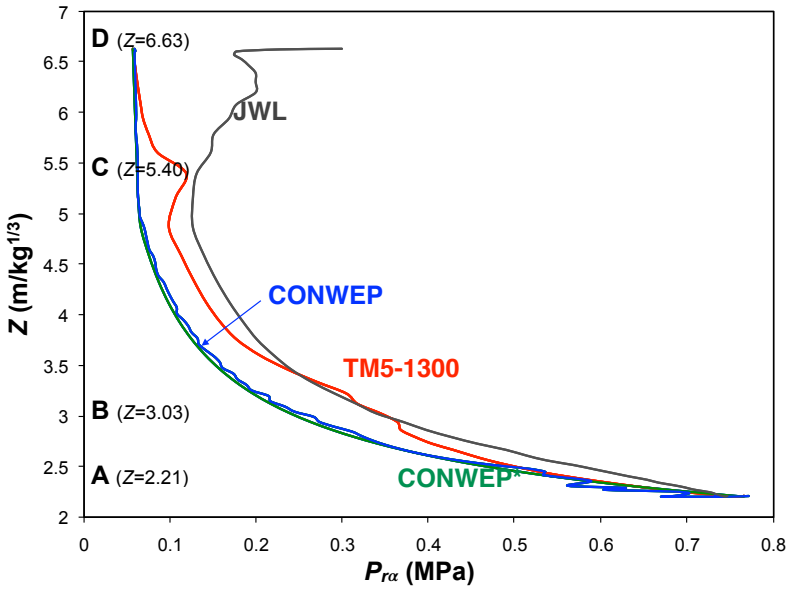

Figure 20: Comparison of $P_{r\alpha}$ as obtained by the four models.

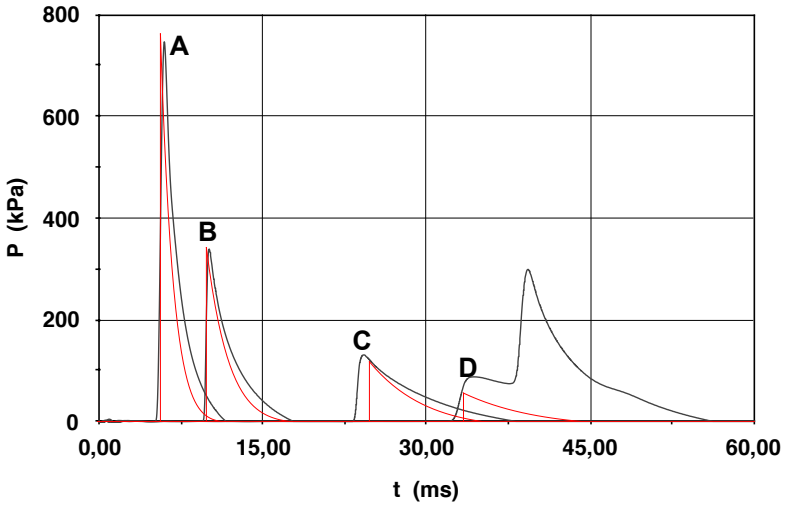

Figure 21: Comparison of the positive phases for points A, B, C and D as given by JWL (black) and TM5-1300 (red).

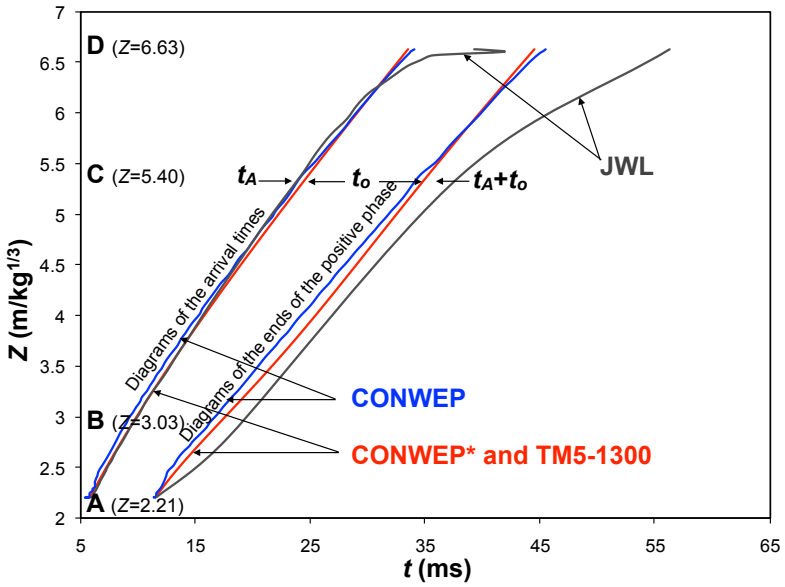

Figure 22: Comparison of the arrival time t_A and of the positive phase duration t_o as obtained by the four models.

7.5 The decay coefficient

A point that can be raised, is the assessment of the decay coefficient b in the Friedlander's equation (5). We have seen that in the procedure detailed in Sect. 5.2, we propose to calculate b as the solution of eq. (28) once $P_{r\alpha}, i_{r\alpha}$ and t_o determined using their respective analytical expressions given in Sect. 4.1.

Of course, such an estimation of b should be validated. To this purpose, let us consider again Fig. 21: we observe that the peaks A, B and C as evaluated by JWL and TM5-1300 are in a rather good agreement (this is not the case for peak D, due to the already remarked effect of focused reflected waves, that of course completely invalidate a Friedlander's type decay). The red curves, relative to TM5-1300, decrease slightly more rapidly than those of JWL, in black. This means that b is slightly overestimated by the procedure sketched in Sect. 5.2.

We have then compared the value of b with the data of the literature. A recent paper, [Karlos et al., 2016], considers the assessment of the decay coefficient b. There, the authors propose a deep analysis of the problem, presenting different laws for b existing in the literature, and in particular a law of the type (9), for spherical or hemispherical blasts, in both the cases for the incident and reflected overpressure. Also in [Ullah et al., 2017] different expressions for b are given. We have then considered such analytical expressions, but we have found a great dispersion of the results, which renders the comparison difficult to be done in a reliable way.

So, we have just compared our results with those given by the law proposed by Karlos et al. in [Karlos et al., 2016]. The comparison is shown in Fig. 23 for the reflected pressure, hemispherical blasts. It shows a good agreement between the two estimations of b and, considering the incertitude of the tests on b due to the difficulty of experimental measures, we can conclude on the validity of the way proposed in Sect. 5.2 for evaluating b.

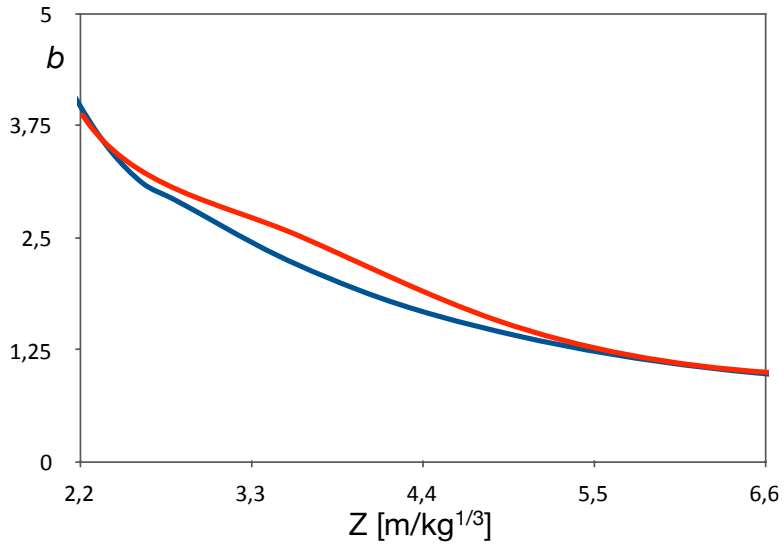

Figure 23: Comparison of the decay coefficient for the reflected pressure, hemispherical blasts, as evaluated by the procedure in Sect. 5.2, red curve, and after [Karlos et al., 2016], blue curve.

8 Conclusion

The results of the simple example treated above clearly show that the distribution of the pressures given by TM5-1300 is sensibly similar to that given by the more exact JWL model, apart from those zones where the interaction of the reflected waves alters the overpressure distribution. This phenomenon, as already explained, strongly depends upon the geometry and the dimensions of the structure and cannot be predicted *a priori*. Simulations done with the JWL model are hence the best way to predict the effects of an explosion, especially when the analysis concerns monumental structures, which involve non-typical geometries that promote multiple reflections and the concentration of the blast energy to specific places and structural elements.

However, the use of JWL can be impractical in the case of very large structures: the need of discretizing finely not only the structure but, even more, the explosive charge and the volume of air can be really problematic for some studies. That is why the use of empirical models, like TM5-1300 and CONWEP, can be very useful in such cases. If abstraction is made concerning the effect of reflected waves, the results of TM5-1300, though obtained neglecting the dynamic pressure, are close to those of JWL, which confirms that the dynamic pressure can be neglected in simulations.

The comparison made of CONWEP, TM5-1300 and JWL confirms what usually stated in the literature: TM5-1300 is more accurate than CONWEP. Nevertheless, as mentioned above, it is this last model that normally is implemented in commercial finite element codes. Its use must hence be accurately considered, adopting a multiplying factor $p_f > 1$. Such a coefficient, affecting only the reflected pressure $P_{r\alpha}$ and not the other blast parameters, namely t_A and t_o, is needed to obtain values that are similar to those predicted by TM 5-1300 and JWL; it represents hence, on the average, the ratio between the value of $P_{r\alpha}$ given by JWL and that given by CONWEP. This coefficient must be chosen in function of the problem at hand, namely considering the characteristic dimensions of the

building: as apparent from Fig. 20, p_f depends upon Z, hence upon R, and upon the angle α. For monuments of large dimensions, we can suggest a value in the interval $1.5 \div 2.5$, in order to take into account, though indirectly, of the effect of reflected waves.

In this paper, we have also proposed new analytical expressions for the representation of the Kingery and Bulmash experimental data on hemispherical blasts. These expressions are really accurate and have the advantage of representing the different physical parameters of a blast over the entire range of variation of the scaled distance Z.

References

T. H. Birhane. Blast analysis of railway masonry bridges. Master's thesis, University of Minho, Portugal, 2009.

H. Draganic and V. Sigmund. Blast loading on structures. *Technical Gazette (Croatia)*, 19:643–652, 2012.

J. W. Strutton - Lord Rayleigh. The problem of the whispering gallery. *Philosophical Magazine, Series 6*, 20:1001–1004, 1910.

J. W. Strutton - Lord Rayleigh. Further applications of Bessel's functions of high order to the whispering gallery and allied problems. *Philosophical Magazine, Series 6*, 27: 100–109, 1914.

H. Jones and A. R. Miller. The detonation of solid explosives. *Proc. Royal Soc. A*, 194: 480, 1948.

V. Karlos and G. Solomos. Calculation of Blast Loads for Application to Structural Components. Technical report, Joint Research Center of the European Commission - Institute for the Protection and Security of the Citizen, Ispra, Italy, 2013.

V. Karlos, G. Solomos, and M. Larcher. Analysis of the blast wave decay coefficient using the Kingery–Bulmash data. *International Journal of Protective Structures*, 7:409–429, 2016.

C. N. Kingery and G. Bulmash. Technical report ARBRL-TR-02555: Air blast parameters from TNT spherical air burst and hemispherical burst. Technical report, U.S. Army Ballistic Research Laboratory, Aberdeen, MD, 1984.

Z. Koccaz, F. Sutcu, and N. Torunbalci. Architectural and structural design for blast resistant structures. In *Proc. of 14th World Conference on Earthquake Engineering*, Beijing, 2008.

E.L. Lee, H.C. Horning, and J.W. Kury. Adiabatic expansion of high explosives detonation products. Technical Report TID 4500 - UCRL 50422, Lawrence Livermore National Laboratory, Liveermore, CA, 1968.

T. Ngo, P. Mendis, A. Gupta, and J. Ramsay. Blast loading and blast effects on structures - An overview. *Electronic Journal of Structural Engineering*, Special Issue: Loading on Structures:76–91, 2007.

A. M. Remennikov. A review of methods for predicting bomb effects on buildings. *J of Battlefield Techn*, 6:5–10, 2003.

M. M. Swisdak. Simplified Kingery airblast calculations. Technical report, DTIC - Defense Technical Information Center, Naval Surface Warfare Center - Indian Head Division, MD, 1994.

A. Ullah, F. Ahmad, H.-W. Jang, S.-W. Kim, and J.-W. Hong. Review of analytical and empirical estimations for incident blast pressure. *KSCE Journal of Civil Engineering*, 21:2211–2225, 2017.

UNODA. International Ammunition Technical Guideline - IATG 01.80: Formulae for ammunition management (2nd Edition). Technical report, United Nations Office for Disarmement Affairs, New York, NY, 2015.

USACE. TM 5-855-1: Design and Analysis of Hardened Structures to Conventional Weapons Effects. Technical report, U. S. Army, 1986.

USACE. TM 5-1300: Structures to Resist the Effects of Accidental Explosions. Technical report, U.S. Army, 1990.

USACE. UFC 3-340-02: Structures to Resist the Effects of Accidental Explosions. Technical report, U.S. Army, 2008.

M. L. Wilkins. The equation of state of PBX 9404 and LX 04-01. Technical Report UCRL - 7797, Lawrence Radiation Laboratory, Berkeley, CA, 1964.